SCIENCE CHINA
Technological Sciences

Special Topic: Functional Materials
• **Review** •

July 2016 Vol.59 No.7: 989–1006
doi: 10.1007/s11431-016-6056-8

The rising star in photovoltaics-perovskite solar cells: The past, present and future

FANG Rui, ZHANG WenJun, ZHANG ShaSha & CHEN Wei*

Michael Grätzel Centre for Mesoscopic Solar Cells, Wuhan National Laboratory for Optoelectronics, Huazhong University of Science and Technology, Wuhan 430074, China

Received February 12, 2016; accepted March 30, 2016; published online June 17, 2016

Perovskite solar cell (PVSC), after its invention since 2009, has attracted tremendous attention from both academia and industry, because of its low cost, ease of manufacturing features and the sky-rocketing efficiencies being achieved within such a short period of time. Currently, the new efficiency record has reached 21.0%, comparable to that of the commercialized PV technologies developed for decades, such as multi-crystalline Si, CIGS and CdTe thin film solar cells. It is very possible that PVSCs would one day step over the threshold of marketization, share or even overturn the current PV market dominated by crystalline-Si solar cells. However, there are still several obstacles to be overcome on the road towards PVSC industrialization. This paper has reviewed the brief developing history and the current research status of PVSCs, and explained: Why PVSCs are so important in the next-generation solar cells, why organometal halide perovskites work so well as light absorbers, and what the inherent differences are among different cell configurations. The prospects on how to realize scale-up industrialization of PVSCs have also been given in the sequence of efficiency, stability, cost, toxicity, and short-term objectives. Resolutions to the remaining challenges according to their orders of technical difficulty and importance have also been discussed.

organometal halides, perovskite solar cells, cell configurations, efficiency records, stability, industrialization prospects

Citation: Fang R, Zhang W J, Zhang S S, et al. The rising star in photovoltaics-perovskite solar cells: The past, present and future. Sci China Tech Sci, 2016, 59: 989–1006, doi: 10.1007/s11431-016-6056-8

1 Introduction

Up to date, ~80% primary energy consumption in the world is provided by fossil fuels, consisting of coal 20.8%, natural gas 31.6%, crude oil 22.3% and NGPL (Natural gas plant liquids) 4.9% [1]. The lacking storage of these fossil fuels, as well as the rise of air pollution/global warming mainly derived from their burning, makes up a strong driving force to develop clean and renewable energies. From Figure 1, it is known that though we have many alternative renewables, such as wave, geothermal, hydro, biomass, wind, and solar, only wind and solar are abundant enough to cover the whole need of today's world energy consumption (16 TW per year). Especially for solar energy, its yearly potential is as high as 23000 TW, implying that only 1% area of the earth with installation of PV module with 10% efficiency would be enough to meet the global energy demand. Indeed, solar power (mostly solar PV) was the leading technology in renewable energy investment during recent years, which accounted for more than 55% of new investment in 2014 [2]. However, the world's PV capacity just reached 200 GW in 2015 [3], only occupying 1% of worldwide electricity demand. Obviously, there is an enormous gap between the theoretical potential and the realistic status of solar PV. How to compensate this gap? The turning point will rest with when and how the levelized energy cost (LEO) of solar PV becomes lower than that of fossil fuels.

*Corresponding author (email: wnlochenwei@hust.edu.cn)

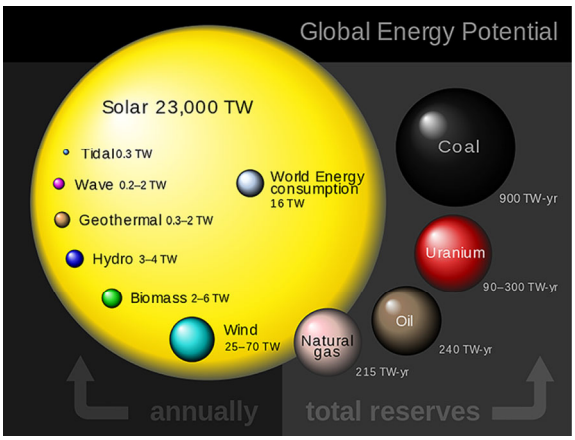

Figure 1 (Color online) Comparison of finite and renewable planetary energy reserves (Terawatt-years). Total recoverable reserves are shown for the finite resources. Yearly potentials are shown for the renewables [2].

The consequent question is: Can the currently commercialized PV technologies someday meet the requirement on LEO? As is known, the up-to-date existing PV technologies could be roughly defined to three generations. The first generation of crystalline silicon (c-Si) solar cells possesses the longest research history and is the most mature in technique, which currently dominates roughly 90% of the PV market. Its price has fallen dramatically from $76.67 per watt in 1977 to $0.30 per watt in 2015. Chinese producers started to join in the supply chain since 2008 and played a very important role in the subsequent price sharp decline. It is possible for c-Si PVs to further decrease the price to some extent through commercial competition and technical improvement, however, the energy-intensive manufacturing processes for high purity (>99.9995%) silicon ingots and solar panels will be the serious challenges [4–7]. The second generation of thin film PVs, including cadmium telluride (CdTe) and copper indium gallium selenide (CIGS) solar cells, shared roughly 10% of the PV market. Their technical limitations are complex and some of them are intrinsic. First and foremost, limitation on the source materials' abundance of Te in CdTe solar cell and In in CIGS solar cell will restrict the up-limit capacities of these two kinds of PVs. For example, one gigawatt (GW) of CdTe PV modules would require about 93 tons of Te, while the global production of Te is estimated to be about 800 tons per year, representing <10 GW/year capacity of CdTe PV modules [8,9]. Similarly, the annual production of In in the whole world could only afford <100 GW/year capacity of CIGS PV modules [10,11]. Second, the toxic Cd element existing in the both kinds of PVs will arouse environmental issues. Third, CIGS is a quaternary compound, whose processing is complex and expensive [12–16]. In short, high materials/processing cost, low crustal abundance, and other technical limitations make the first and second generations of solar cells very hard to substitute fossil fuels on a large scale. And predictably, this circumstance would not change in a long term.

Higher possibility is only buried in the next generation (also termed as the third generation) of solar cells on the basis of totally different materials/technologies. That is also the direct driving force for the worldwide researchers to develop alternative PV technologies with lower cost and higher efficiency. The emerging PVs reported to date include dye-sensitized solar cell, quantum dot solar cell, CZTS solar cell, organic solar cell and perovskite solar cell (PVSC) (Figure 2) [17]. Most of them have reached efficiencies of more than 10%. Although it is still much lower than the threshold level to enter market competition, no one could deny that those emerging technologies have big potentials in the future, since their developing histories are much shorter than the commercialized PVs. Among them, PVSC outshines others, at least in the efficiency evolution. Though PVSC only appeared 6 years ago, its efficiency record has been dramatically improved from 3.8% to be 21.0% [17–20], nearly the same as that of multi-crystalline silicon (21.25%), CIGS (21.7%), and CdTe (21.5%) solar cells which were realized after decades of development [21].

Why did PVSCs make so fast progress? Will PVSCs be a game changer in the near future? What is the main obstacle for the future industrialization of this kind of technology? In this paper, these above items will be reviewed and discussed; and some viewpoints are proposed according to the authors' research experience. Firstly we certified the large area (>1 cm^2) PVSC with a record efficiency in the accredited certification laboratory of the National Institute of Advanced Industrial Science and Technology (AIST) in Japan [22].

2 Organometal halides-an ideal light harvester

Perovskite is named after a Russian mineralogist Lev Perovski for the memory of his discovery of the mineral $CaTiO_3$ in the Ural Mountains of Russia in 1839. It represents a series of compounds sharing the same type of crystal structure as $CaTiO_3$ (Figure 3) [23]. Compounds with the perovskite structure include not only oxides, but also some carbides ($MgCNi_3$) [24], nitrides ($TaThN_3$) [25], halides ($NaMgF_3$), and hydrides ($NaMgH_3$) [26]. The perovskites used as light absorbers in solar cells are typically organometal halides with general formula of ABX_3, where typically A = $CH_3NH_3^+$, NH_2-CH_2=NH_2^+; B = Pb^{2+}, Sn^{2+}; and X = Cl^-, Br^-, I^-. As far the most efficient perovskites are $CH_3NH_3PbI_3$ ($MAPbI_3$) and NH_2-CH=NH_2PbI_3 ($FAPbI_3$).

2.1 Crystal structure

The ideal perovskite-type structure is 3-D cubic with general formula of ABX_3 [27]. Depending on the relative ionic radii of A, B, X site ions (denoted as r_A, r_B, r_X), the structure could be less symmetric tetragonal or orthorhombic. A tolerance factor (t-value) defined by the equation below

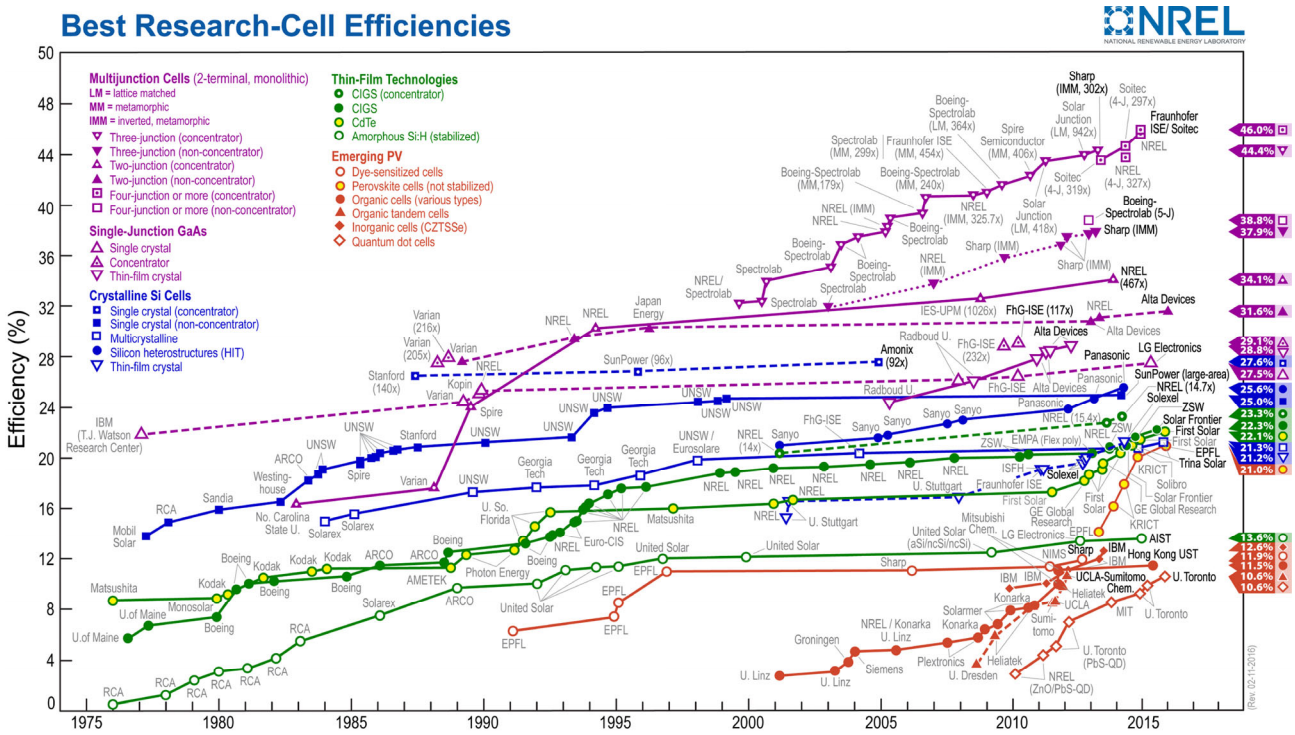

Figure 2 (Color online) Best research-cell efficiencies collected by National Renewable Energy Laboratory (NREL) [17].

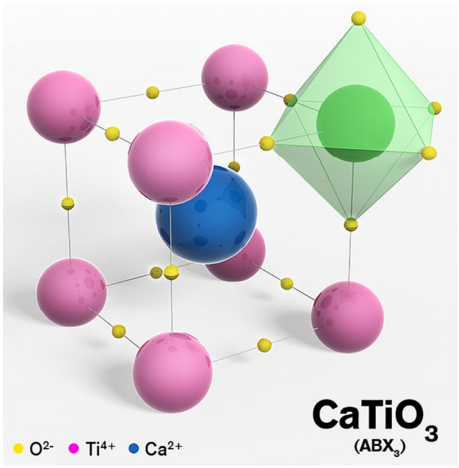

Figure 3 (Color online) The perovskite structure compounds sharing the same crystal structure as $CaTiO_3$ [23].

could be employed as the criterion to judge whether the ideal 3-D perovskite structure could be present or not.

$$t = \frac{r_A + r_B}{\sqrt{2}(r_B + r_X)}.$$

For oxide perovskites, allowable t-values are in the range of $0.75 < t < 1$; while for halides perovskites, they are in the range of $0.85 < t < 1.11$, and only for t within the narrower range of 0.89–1.0, the desired cubic crystal symmetry could be achieved [28,29].

Another important factor, the octahedral factor (μ), is defined as the relative ratio of B site and X site ionic radii, r_B/r_X [30–32], which is necessary for the prediction of perovskite formation. When μ is below 0.442 (0.425 for oxide perovskites), the octahedron BX_6 will be unstable [29,33]. Referring to t and μ shown in Figure 4 [34], 12 organometal halide perovskites with A site cations of $CH_3CH_2NH_3^+$ (EA^+, $r_A = 0.23$ nm) and $CH_3NH_3^+$ (MA^+, $r_A = 0.18$ nm), B site cations of Pb^{2+} ($r_B = 0.119$ nm) and Sn^{2+} ($r_B = 0.110$ nm), and X site anions of Cl^- ($r_X = 0.181$ nm), Br^- ($r_X = 0.196$ nm) and I^- ($r_X = 0.220$ nm), respectively, their crystal structures and structural stability could be accordingly predicted.

2.2 Photoelectric properties

2.2.1 *Tunable bandgaps*

The bandgaps of ABX_3 perovskites have been demonstrated

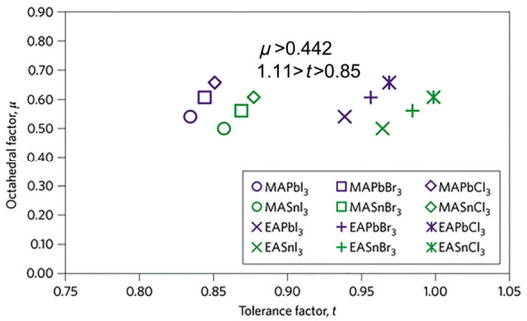

Figure 4 (Color online) Match t and μ for 12 halides perovskites with given parameters [34].

to be easily tenable via simply changing the materials' compositions [35–37]. This is a great benefit for light absorbers in photovoltaic cells because it allows design and optimization of devices more flexibly. In particular, it could produce different translucent colors, which enables the realization of colorful solar cells for solar window applications [38]. As demonstrated in the literatures [39–41], bandgaps of $MAPb(I_{1-x}Br_x)_{3-y}Cl_y$ series perovskites could be tuned ranging between 1.58–2.29 eV by changing the ratios of halide anions [39]; bandgaps of $MASnI_{3-x}Br_x$ series perovskites could be controlled in the range of 1.30–2.15 eV by changing ratios of Br^-/I^- [37,41], and bandgaps of $MAPb_{3-x}Sn_xI_3$ could be controlled in the range of 1.17–1.55 eV by changing ratios of Pb^{2+}/Sn^{2+} [42].

Note that, according to the Shockley-Queisser limit for a single junction solar cell, the optimal bandgap referring to the maximum theoretical efficiency of 33.7% is 1.37 eV [43]. As far, the most successful perovskites $MAPbI_3$, with a bandgap of 1.55 eV [44–47], correspond to an efficiency up-limit of 31.3%, and $FAPbI_3$ with a more favorable bandgap of 1.47 eV [47–49] could result in a higher efficiency up-limit of 32.5%.

2.2.2 *Optical absorption*

As the essential parameters of light harvesters, both the light absorption range (related to bandgap [50]) and the absorption coefficient (for direct bandgap semiconductor up to 5×10^5 cm^{-1} [34]) play important roles for the solar cell applications [38,51,52].

First, by integrating the product of incident photon flux density and incident photon-to-electron conversion efficiency (IPCE) over the wavelength (λ) of the incident light, short-circuit photocurrent density (J_{SC}) of a solar cell can be obtained by the following equation:

$$J_{SC} = \int q \times F(\lambda) \times \mathrm{IPCE}(\lambda) \times \mathrm{d}\lambda,$$

where q is the electron charge, and $F(\lambda)$ is the incident photon flux density at the wavelength of λ [53]. As a consequence, both λ and IPCE(λ) are determining factors in a given incident light for J_{SC}. It is clear that wider light absorption range will result in a higher J_{SC}. The absorption spectra of $MAPb(I_{1-x}Br_x)_3$ and $MASn_xPb_{(1-x)}I_3$ films varying with x values are shown in Figure 5(a) [37] and (c) [34], respectively. The absorption edge blue shifts from 800 to 540 nm after adding Br^- ions to the $MAPb(I_{1-x}Br_x)_3$ series films, manifesting as the films' color varies from black to yellow (Figure 5(b)) [50]. While Pb is replaced by Sn in the $MASn_xPb_{(1-x)}I_3$ series films, the absorption edge is extended to the near-infrared region (up to 1060 nm), which is necessary to realize high-efficiency tandem PVSCs [54–57].

Besides, higher absorption coefficient needs a very small thickness of active film to fully capture the incident solar light, therefore shorten the charge transport paths and benefit for higher charge collection efficiency. As shown in Figure 5(d), the perovskites present very high absorption coefficients of 10^{-4}–10^{-5} cm^{-1} in the visible region and very sharp absorption edges associated with their direct bandgap characteristics. These are comparable to most of the classic semiconductors applied in thin film solar cells, e.g., CIGS, CdTe, GaAs, etc. [34], but much different from the indirect bandgap c-Si with much lower absorption coefficient (10^{-3} cm^{-1}) and long week absorption tail in the near-IR region. As is known, high performance c-Si solar cell requires very high purity (>99.9995) source material to make sure the effective charge transport length can exceed the long optical length of ~180 microns, which is decided by its optical absorption characteristics.

2.2.3 *Charge transport*

Beyond light absorption, the effective charge diffusion length (L) is another key factor determining the device performance, which is associated with charge separation/collection. It is determined by carrier lifetime (τ) and diffusion constants (D) as the equation of $L=\sqrt{D\tau}$ [47,58–63]. By monitoring the time-resolved photoluminescence intensity, Xing et al. [58] got the balanced charge diffusion lengths of $MAPbI_3$ film in the order of ~100 nm. It has been firstly recognized that both electrons and holes have balanced and long diffusion lengths in the $MAPbI_3$ film, which holds the key for the efficient operation of diverse configurations of PVSCs. Samuel et al. [59] found a much longer diffusion length of ~1 μm in the $MAPbI_{3-x}Cl_x$ film, in which the Cl^- dopant was suggested to benefit for a

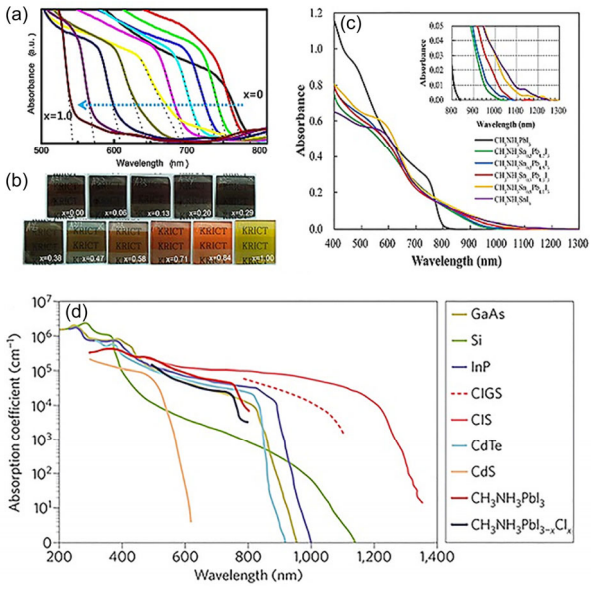

Figure 5 (a) UV–Vis absorption spectra of the $MAPb(I_{1-x}Br_x)_3$ series films; (b) photographs of the corresponding films in (a) [37]; (c) absorption spectra of the $MASn_xPb_{(1-x)}I_3$ series films [50]; (d) absorption coefficients of $MAPbI_3$ and $MAPbI_{3-x}Cl_x$ films; some other classic semiconductors in PVs are shown together for comparison [34].

substantial inhibition of non-radiative electron-hole recombination. Yet the intrinsic role of Cl^- dopant in the $MAPbI_{3-x}Cl_x$ film is still under debate [64–67]. The dissenters thought the difference in ionic radii between Cl^- and I^- was too large for the cubic perovskite crystal structure to provide any doping tolerance for Cl^- [45]. Besides, the amount of the residue Cl^- ions in the $MAPbI_{3-x}Cl_x$ film and their exact location in the crystal domains are also not clear. These above are also normally cited as the objections by the dissenters. According to our experience, in the very beginning Cl^- dopant strategy may be important to improve the perovskite film quality (less pin-holes and larger domain size), which may be sufficient to explain its longer diffusion length. It is suggested that many film preparation details could result in film quality tuning, which will result in different charge diffusion coefficients and lifetimes of the perovskite films. The important variables could be: (1) the source materials' purity [68], (2) the deviation from the ideal stoichiometric ratio [69–72], (3) the film morphology associated with preparation methods [73–75], and (4) the possible presence of new interphase during post annealing of perovskite films [48,76]. Recently, the best-in-class PVSCs based on >300 nm thick $MAPbI_3$ films [22,48] have shown ~90% IPCEs, meaning negligible charge collection losses and long effective diffusion lengths at least over 300 nm. We think it should be closely related to the better film quality of $MAPbI_3$ resulting from the improved film preparation methods [22].

Recently, Dong et al. [63] revised the effective diffusion length up to 175 μm in bulk single crystal of $MAPbI_3$, which further manifested the importance of material's quality for its charge transport properties. The remarkable long diffusion length is suggested to result from greater carrier mobility (105 ± 35 $cm^2\ V^{-1}\ s^{-1}$ for holes and 24.0 ± 6.8 $cm^2\ V^{-1}\ s^{-1}$ for electrons), longer lifetime (95 ± 8 μs), and much smaller trap densities ($3.6 \times 10^{10}\ cm^{-3}$) in the single crystal than that in polycrystalline thin films. Herein, the effective diffusion length is determined by

$$L = \sqrt{\frac{k_B T \mu \tau}{e}},$$

where k_B, T, μ, τ and e are the Boltzmann constant, absolute temperature, carrier mobility, carrier lifetime and elementary charge, respectively.

Significant imbalance in diffusion lengths between holes and electrons in $FAPbI_3$ was found by Eperon et al. [47], which was ascribed to the lower diffusion coefficient for electrons rather than the reduced lifetime. The unbalanced charge transport between holes and electrons could be an important reason for the infamous hysteresis in the reported devices [77–79].

Several classic photovoltaic semiconductors, e.g., CIGS [80], GaAs [81], c-Si [82], etc., are also included in Table 1 for comparison. It is clear that the charge transport properties of perovskite films or single crystal prepared by low temperature solution process can catch up with or even be superior to that of c-Si, CIGS and GaAs thin films prepared by very expensive and energy-intensive techniques.

3 Devices

PVSCs, only after 3 years of the first solid-state device being reported in 2012, have presented diverse cell configurations with high performance. A consequent question is: is there any intrinsic advantage of a certain cell configuration over others?

As shown in Figure 6, diverse cell configurations could be generally divided into 3 main branches according to their intrinsic difference in working principle. The first branch is derived from dye-sensitized solar cells, which embodies a mesoscopic electron injection interface normally made of nanocrystalline TiO_2 and could be called "regular mesoscopic structure". To date, the most efficient PVSCs reported by Seok's group [48] and Gratzel's group [83] with certified efficiencies of ~20% still employed a very thin (~150 nm) mesoporous TiO_2 scaffold. Note that in such a

Table 1 The essential charge transport properties of perovskite films and single crystal, some classic photovoltaic semiconductors are included for comparison

PV semiconductors	Species	D ($cm^2\ s^{-1}$)/μ ($cm^2\ V^{-1}\ s^{-1}$)	L (nm)	Ref.
$MAPbI_3$ (thin film)	Holes	D: 0.017±0.011	129±41	[58,59]
	Electrons	D: 0.011±0.007	105±32	
$MAPbCl_3$ (thin film)	Holes	D: 0.042±0.016	1069±204	[59]
	Electrons	D: 0.054±0.022	1213±243	
$FAPbI_3$ (thin film)	Holes	D: 0.091±0.009	813±72	[47]
	Electrons	D: 0.004±0.001	177±20	
$MAPbI_3$ (single crystal)	Holes	μ: 165±25	175±25 μm	[63]
CIGS	Electrons	μ: 100	0.91 μm	[80]
GaAs	Holes	μ: 6500	~20 μm	[81]
mono-Si	Electrons	μ: 1400	147 μm	[82]

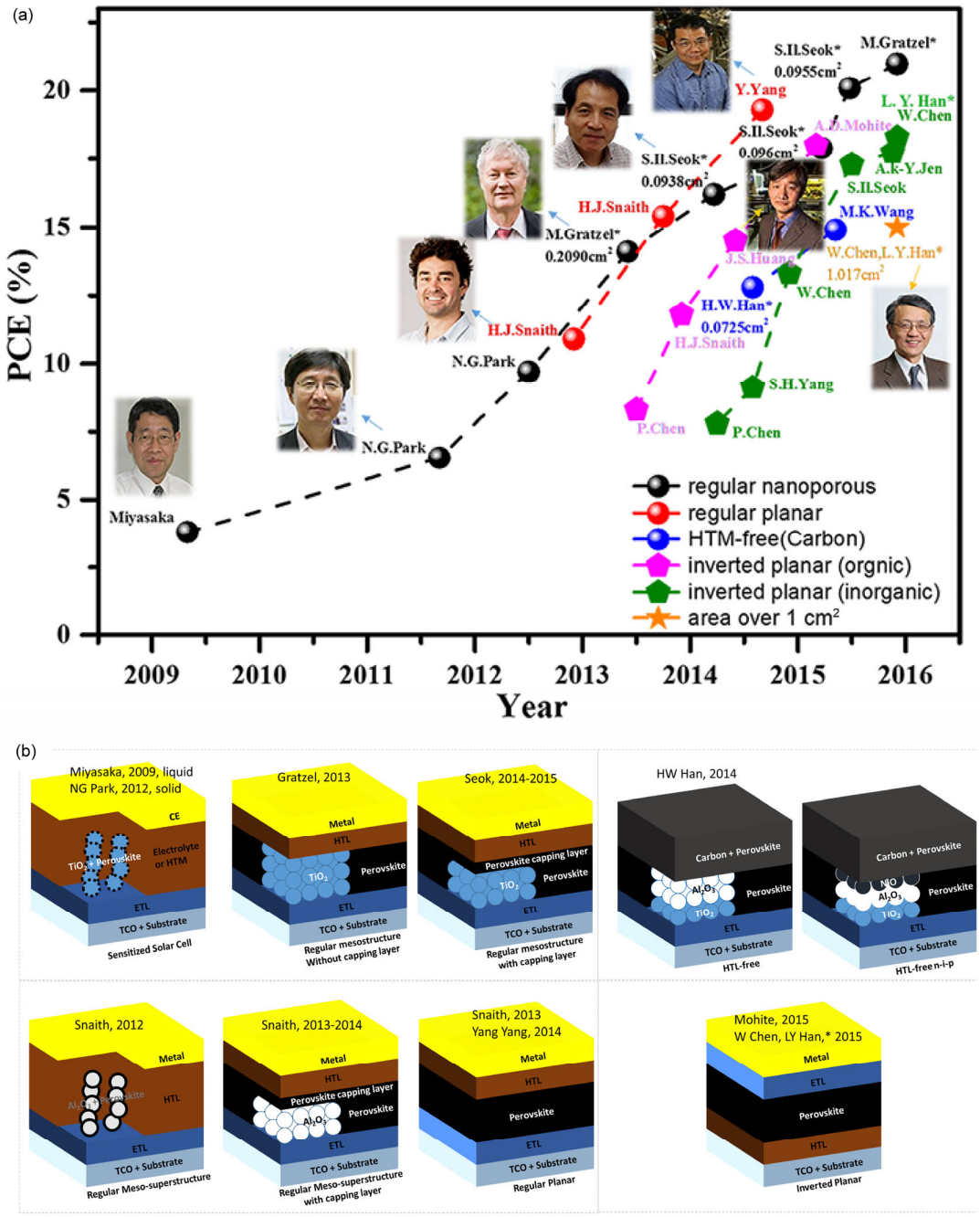

Figure 6 (Color online) (a) Summary on the landmark progress of PVSCs: the efficiency evolution of PVSCs with different cell configurations; the photographs of some representative researchers in this field are shown as the insets, (b) structural evolution of PVSCs. ETL, electron transport material; HTL, hole transport material.

configuration, n-type selective contact (normally compact TiO_2) is located in the bottom and the photo-generated electrons are collected by the front TCO glass. The second branch is called "regular planar structure", of which the current flow direction is the same as the first branch, but without the mesoporous TiO_2 scaffold for electron collection. This cell configuration has been reported with the best efficiency of 19.3% by Zhou et al. [84]. However, the efficiency has not been certified and the associated device has been reported with evident hysteresis. Liu et al. [85] employed a mesoporous Al_2O_3 scaffold in their so-called "meso-superstructured" PVSC, which could actually be included in the "regular planar structure" branch, because the insulated Al_2O_3 has no evident electrical function in such a device. The third branch is the "inverted planar structure", which employed a compact p-type hole selective layer in the bottom. The current flow direction in such kind device is photo-generated holes being collected by the front TCO glass. Note in Figure 6, we divide the "inverted planar structure" into two sub-branches for easier comparison: one

is the inverted planar "organic" which is based on organic hole selective contact normally made of PEDOT: PSS [86–90]; the other one is the inverted planar "inorganic" which is based on an inorganic hole selective contact normally made of NiO_x [22,91–97]. The inverted planar structure is normally reported with small hysteresis. Recently the corresponding author of this paper has certified the first large area (>1 cm^2) PVSC with record efficiency of 15%, which is also based on this cell configuration [22].

3.1 Regular meso-structure

This cell configuration is favored by researchers on the dye-sensitized solar cells involving mesoporous TiO_2. The working mechanism was initially copied from the solid-state dye-sensitized solar cells. In 2009, Kojima et al. [98] reported the first PVSC using such a cell configuration, in which ultrafine $MAPbI_3$ and $MAPbBr_3$ nanoparticles were used as sensitizers decorated on mesoporous TiO_2 film (8 μm for $MAPbI_3$ and 12 μm for $MAPbBr_3$ in thickness). The device stability was very poor owing to the dissolution of perovskites in the liquid electrolyte. That is why this original research got nearly no citation within nearly 3 years after its publication. In 2012, Kim et al. [99] firstly reported a solid-state PVSC using Spiro-OMeTAD as the hole transport material to replace liquid electrolyte and promoted the photo-conversion efficiency (PCE) to 9.7%. The device stability was also largely improved. Note in this cell, the meso-TiO_2 film thickness was ~600 nm, on top of which there was no perovskite capping layer. Afterwards, Julian et al. [100] in 2013 reported the first certified efficiency of 14.14% of PVSC with similar cell configuration. In their work, the meso-TiO_2 film thickness was optimized to be ~350 nm. A two-step method for perovskite preparation, by immersing the pre-deposited PbI_2 film in MAI isopropanol solution, was also reported for the first time in PVSCs. Also, their device has no continuous capping layer of perovskite on top of meso-TiO_2, implying a possible direct contact between TiO_2 and spiro-OMeTAD. This would lead to higher possibility of interfacial recombination and therefore lower V_{OC} of the solar cell (993 mV). What is notable, in recently certified PVSCs by Seok's group, the meso-TiO_2 film thickness was controlled gradually thinner. For example, they firstly certified an efficiency of 16.2% with the cell configuration of "FTO/compact TIO_2/meso-TiO_2 (200 nm)/$MAPbI_3$ capping layer (200 nm)/PTAA(50 nm)/Au". In this device, $MAPbI_3$ film's quality was improved by the anti-solvent drop-casting method. They emphasized the importance of a 200 nm thick $MAPbI_3$ capping layer fully covered on top of the meso-TiO_2. And therefore, the electron transport meso-TiO_2 and hole transport PTAA have no direct contact in spatial. That is why they got improved V_{OC} of 1.06–1.08 V. Besides, they also claimed the presence of meso-TiO_2 layer could help to remove hysteresis [101]. After that, they used hybrid $MAPbBr_3$-$FAPbI_3$ perovskite as light harvester, promoted J_{SC} to 22 mA cm^{-2} and certified PCE of 17.9% [102]. In 2015, they found a new method to produce high-quality $FAPbI_3$ films with a smaller bandgap than $MAPbI_3$. The reported J_{SC} has been increased to 24.7 mA cm^{-2}, and the certified PCE has been elevated to 20.1% [48]. Note that, in this cell, the meso-TiO_2 layer thickness has been decreased to 150 nm. Recently later, Bi et al. [83] in Hagfeldt's group in EPFL reported a 20.8% PCE (19.9% certified PCE) based on similar cell structure with a 150 nm meso-TiO_2 layer and a $MAPbBr_3$-$FAPbI_3$ mixed perovskite layer. They emphasized the importance of a slight excess of PbI_2 in the perovskite film, which was proved to be useful to decrease recombination and therefore improve V_{OC} up to 1.16 V. Although the excess PbI_2 has been claimed to be with positive effect to the device efficiency [70–72], a paper demonstrated its presence was not good for the long term stability, recently [69]. This might be reasonable, since energy barrier for PbI_2 lattice to admit MA^+ intercalation/deintercalation is very low. The temporary PbI_2 interfacial condition cannot be maintained during long-term working conditions. EPFL recently has refreshed the champion efficiency up to 21.0%, the detailed cell configuration is still waiting for their further disclosure.

3.2 Regular planar-structure

As early as 2012, Michael et al. [103] for the first time proposed the meso-TiO_2 was not necessary for PVSCs. They employed insulated meso-Al_2O_3 to replace the semiconducting meso-TiO_2 in the device with a structure of "FTO/compact TiO_2/meso-Al_2O_3/$MAPbI_3$/Spiro-OMeTAD/Au" and gave a competitive PCE of 10.9%. In 2013, Liu et al. [85] moved forwards to fully planar structure of "FTO/compact TiO_2/$MAPbI_3$/Spiro-OMeTAD/Au" and demonstrated a 15% PCE. The major improvement is their perovskite film quality prepared by co-thermal evaporation of MAI and PbI_2. Though later, other researchers including Sniath disclosed that the regular planar structure devices generally had hysteresis problem [104,105]. The reported performance obtained from one certain scanning direction could be largely overestimated. In 2014, Zhou et al. [84] reported a high PCE of 19.3% with the regular planar cell structure. Their work emphasized the importance of interface engineering to the device performance, such as controlling the formation of perovskite film to suppress carrier recombination, and improving conductivity of interface layer to facilitate carrier extraction. They stated their device was not stable neither in air nor in N_2 atmosphere, and the PCE obtained from the regular scanning direction was ~3% lower in absolute PCE value than that from reverse scanning direction.

The inherent reason, why regular planar devices presented more serious hysteresis than that of regular mesoscopic devices, is still under debate. Chen et al. [106] claimed the presence of meso-TiO_2 scaffold led to disper-

sive ferroelectric polarization of $MAPbI_3$ domains under certain external bias, which recovered much easier during the I-V measurement than that in the planar device without such a scaffold layer [107]. While Wu et al. [108] proposed there was an unfavorable energy barrier present between planar heterojunction of TiO_2/$MAPbI_3$, because they had not monitored any PL quenching between them. To our viewpoint, the unbalanced charge extraction may hold the key for different hysteresis associated with device structure. The presence of meso-TiO_2 scaffold will extract photo-induced electrons from $MAPbI_3$ within nanoseconds. And then, electrons transport through meso-TiO_2 network within micron seconds. Note that, the diffusion coefficient of the meso-TiO_2 film is normally reported on the order of 10^{-4} $cm^2\ s^{-1}$ [109], slower than that of $MAPbI_3$ with diffusion coefficient of $>10^{-2}$ $cm^2\ s^{-1}$ [59]. That means the presence of meso-TiO_2 in the regular mesoscopic device is to slow down rather not speed up the overall electron transport. It may help to balance the electron and hole transport within the device. While in the regular planar device, charge transport becomes unbalanced and leads to accumulation of one-sort of charges. A recent paper using electro-optical analysis has revealed that charge accumulation will strongly distort the perovskite structure at the interface and cause pronounced hysteresis [108]. It is interesting that the champion efficiency holder, Shin et al. [110] at KRICT, recently reported to use Zn_2SnO_4 compact layer to replace TiO_2 compact layer in regular planar PVSC. However, the I-V hysteresis has not been removed in the device. Does that imply hysteresis cannot be removed in regular planar PVSCs? If it is so, what is the inherent mechanism? This still remains an open question worthy for in-depth research in the future.

3.3 Inverted planar-structure

Unlike regular devices, inverted PVSCs normally have no p-type mesoporous scaffold, with a planar structure. The hole transport materials in inverted PVSCs could be PEDOT: PSS, NiO, MoO_3, V_2O_5 and WO_3.

PEDOT: PSS is a standard component in organic solar cells. The first inverted planar PVSC also used PEDOT: PSS as the hole transport material [87]. Up to date, the reported performance of PEDOT: PSS based inverted PVSCs have been steadily improved to ~18% [88–90]. Among those reports, a "Science" paper claimed their 18% PCE was achieved by employing higher quality of $MAPbI_3$ films with millimeter domain sizes [89]. Yet many researchers argued that the apparent domains in their film were not made of real single crystals. Up to now, to the best of our knowledge, the highest certified efficiency for PEDOT: PSS based inverted PVSC is 15.3%, with J_{SC} of 19.8 mA cm^{-2}, V_{OC} of 0.936 V and *FF* of 0.832, which is achieved by a Taiwan research group [90]. To date, most of the PEDOT: PSS based inverted PVSCs represented hysteresis free in their I-V curves and remarkably high *FF* of > 0.8, which are their notable advantages over regular PVSCs. However, the intrinsic problem is that the relatively low work function of PEDOT: PSS has limited V_{OC} below 1 V, which is about 0.1 V lower than the best regular PVSCs. Note that the conductivity of PEDOT: PSS (10^2–10^3 S cm^{-1}) is much higher than that of spiro-OMeTAD (10^{-3}–10^{-4} S cm^{-1}), and the resistance of PCBM layer with thickness of 60 nm should be also lower than that of meso-TiO_2 film with thickness of > 150 nm [111]. Therefore, it is reasonable that the inverted PVSCs have higher *FF* due to the obviously lower interfacial charge transport resistances. Besides, the planar device has the minimized interfacial contacts, which in principle benefits for controlling the interfacial recombination loss. Higher conductivity of interfacial layers also results in fast charge extraction with no charge accumulation at the interfaces, which is also benefit for hysteresis free of the device.

Transition metal oxides, such as NiO, MoO_3, V_2O_5 and WO_3, have also been exploited as hole transport materials in organic solar cells [112,113]. They were mostly reported with higher stability than the organic counterpart of PEDOT: PSS. While in PVSCs, the primary purpose is to utilize their higher work functions to get higher V_{OC}. Recent literatures demonstrated MoO_3, V_2O_5 and WO_3 be intrinsic n-type semiconductors but with deep-lying electronic states. Their hole selective collection is realized by electron transport through their gap states and recombination with holes from photoactive materials. That is different from NiO, which is an intrinsic p-type semiconductor with a very low E_{CB} which could build an effective energy barrier for electron injection. Up to date, NiO based hole transport materials have been reported frequently and sufficiently optimized in PVSCs [22,91–97,114–116], while MoO_3 [117,118], V_2O_5 [119], and WO_3 [120] have been reported rarely with relatively poor performance.

In the very beginning, Ren et al. [118] employed a cell structure of "ITO/NiO/meso-NiO/$MAPbI_3$/PCBM/BCP/Al" and demonstrated a 9.51% PCE. Not like meso-TiO_2 in the regular mesoscopic PVSCs, the presence of meso-NiO in the inverted PVSCs has been demonstrated without any necessity. About the compact NiO layer, its fabrication methods become diverse, such as sol-gel spin-coating method [115], low-temperature sputtering method [116], NiO nanoink method [94], pulse layer deposition method [96] and spray-pyrolysis method [22,95]. Some general principles to control the quality of NiO interfacial layer have been disclosed: (1) pin-hole free morphology of the compact NiO is associated with the shunt resistance of the solar cells; (2) the intrinsic light absorption of NiO should be controlled as small as possible to minimize the interfacial light absorption loss; (3) the conductivity of NiO should be controlled suitably high, which is associated with the film quality dependent upon preparation techniques and implementation of the doping strategies; and (4) the matchup of its bandgap energy levels with perovskite light absorbers facilitates the hole injection [121]. Note that, (1), (2), and (3) should be taken into comprehensive and balanced consideration. For example, higher thickness normally repre-

sents better coverage on conductive glass substrate, but lower optical transmittance and higher charge transport resistance. The corresponding author of this paper, W. Chen and his coworkers firstly employed a hybrid interfacial layer consisting of a 10–20 nm compact NiO plus a thin meso-Al_2O_3 layer in inverted PVSCs. Such a hybrid interfacial layer featured as both high optical transparency and specific dual blocking effect, leading to minimal light absorption loss and interfacial recombination loss. Finally, 13.5% efficiency has been achieved [95]. Seok and his coworkers prepared highly transparent NiO films through pulsed laser deposition (PLD) with controlled crystallographic orientation. It seems the NiO film quality is higher due to the PLD technique employed. The reported thickness has reached as high as 100 nm, but the film is still transparent and conductive enough. The researcher emphasized the presence of mesoporous structure in their optimized morphology of PLD deposited NiO films, which could facilitate hole extraction [96]. They finally reported a high efficiency of 17.3%. The corresponding author of this paper, W. Chen and his coworkers developed heavily doping inorganic charge extraction layers made of $Ni_{0.80}Mg_{0.15}Li_{0.05}O$ and $Ti_{0.95}Nb_{0.05}O_x$ in inverted planar PVSCs. The doping enhanced conductivities result in a very rapid carrier extraction. Besides, even with 10- to 20-nanometer thickness, it has been demonstrated the pinholes and local structural defects could be avoided over large areas. Thus, a record efficiency of 18.3% and remarkable *FF* of 0.83 have been achieved for the inverted planar PVSC with small area (0.09 cm^2). Besides, the device has been demonstrated with hysteresis free characteristics and good stability over light soaking for 1000 h. All of these guarantee the device with area >1 cm^2 be successfully certified with a high efficiency of 15% by an accredited photovoltaic calibration laboratory, AIST in Japan. It was the first time for PVSCs being certified with such a large area, which filled in the blank of the classic "solar cell efficiency tables" edited regularly by Green et al. [122] and for the first time allowed PVSC to be compared with other PV technologies in the same standard [123]. Note that 18.3% efficiency was only achieved based on $MAPbI_3$. $FAPbI_3$ with narrower bandgap is believed to have higher possibility to get > 20% efficiency in the near future.

3.4 Other structures

Beyond these above main branches, a low-cost mesoscopic cell configuration based on screen-printed mesoporous layers of "meso-TiO_2/meso-ZrO_2/meso-Carbon" [124] has also been raised in Figure 6. In such a device, all of the charge transfer interfaces are mesoscopic. No organic hole transport layer is involved in the device, which should be the main reason for its reported better stability. The pore filling of perovskite into the overlaid mesoporous films with the total thickness of >10 μm should be one of the main obstacles for such kind of device to achieve high PCE. Li et al. [125] employed 5-ammoniumvaleric acid (5-AVA) as the additive in the perovskite solution which largely improved pore filling and meanwhile maintained good photoelectrical properties of the resultant mixed perovskite, $(5\text{-AVA})_x(MA)_{1-x}PbI_3$. They finally demonstrated a certified efficiency of 12.84%. Recently, Xu et al. [126] inserted a p-type meso-NiO layer between meso-ZrO_2 and meso-Carbon to help hole extraction, and finally got a remarkable efficiency of 14.9% (not certified). They suggested that further improvement on the performance of this device should rest with suppression of fast interfacial recombination, which is a common issue in kinds of mesoscopic solar cells. Wei et al. [127] used kinds of novel techniques to prepare planar carbon electrodes on top of perovskite films, such as inkjet printing and rolling transfer candle soot [128], to construct hole conductor free PVSCs with configuration of "meso-TiO_2/perovskite capping layer/planar-Carbon" [129–131]. These studies highlighted the importance of controlling the contact property between planar perovskite and carbon layers. They later applied an improved solvent engineering method to control the perovskite film quality and promote their cell efficiency by up to 10% at a large area of 1 cm^2 [132].

4 Prospects for PVSCs towards industrialization

4.1 Promoting PCE

4.1.1 PCE in laboratory

Improving the efficiency of PVSCs to >25% will strengthen its economic competitiveness. In physics, as defined by the Shockley–Queisser limit, the maximum theoretical efficiency of a single junction solar cell is around 33.7%, assuming light absorber with a bandgap of 1.34 eV (using an AM 1.5 solar spectrum) [43]. Any deviation from the ideal bandgap will result in smaller theoretical efficiency up-limit. Mono-Si with bandgap of 1.1 eV represents a maximum efficiency of 32%, and to date a practical record of 25.6% has been achieved. GaAs with bandgap of 1.43 eV represents a maximum efficiency of 32.7%, and to date a practical record of 28.8% has been achieved. The most important two kinds of perovskites, $MAPbI_3$ and $FAPbI_3$, are reported with bandgaps of 1.55 and 1.47 eV, corresponding to the theoretical maximum efficiencies of 31.3% and 32.5%, respectively, but as far the best-in-class PVSCs just gave 18.3% for $MAPbI_3$ and 20.1% for $FAPbI_3$ [22].

Mono-Si and GaAs solar cells are the two PV technologies whose practical efficiencies approach their theoretical up-limits most. Comparing the performance parameters of PVSCs with those two best references will benefit identifying the big losses in current PVSCs.

As summarized in Table 2, in comparison to other kinds of solar cells with record efficiencies, the biggest loss in PVSCs comes from J_{SC}. Using the light absorption thresholds for theoretical J_{SC} calculation, the practical J_{SC} of PVSCs is ~ 6 mA cm^{-2} lower than their theoretical maximums. Such J_{SC} loss is comparable to that of CIGS solar cells, but much higher than that of mon-Si and GaAs solar cells with the loss value of only 2–2.5 mA cm^{-2}. It is believed there is a big room to boost J_{SC} of PVSCs in the future if the loss mechanisms could be clearly identified first. The optical loss from the front conductive glass (reflection and absorption) accounts for the large part of J_{SC} loss (at least > 3 mA cm^{-2}); meanwhile, light absorption of the front interfacial layer, insufficient absorption in the near-IR region of perovskites, and a little bulk/interfacial recombination account for the other part of J_{SC} loss. Through introducing light trapping structure and antireflection layer [133,134], the optical loss of front conductive glass could be reduced by at least 50%. Meanwhile, developing new perovskites with narrower band gaps and sharp light absorption thresholds, suitably increasing the perovskite film thickness and improving the film quality (larger domain size, lower defects density) [63,89,135] will result in further J_{SC} improvement.

The optimal V_{OC} is suggested to be 0.3 V lower than the bandgaps of light absorbers. 0.3 V is a typical value due to contact loss [136]. V_{OC} loss in GaAs solar cells is very close to 0.3 V, better than that of mono-Si with 0.38 V V_{OC} loss. While the best PVSCs are with about 0.4–0.45 V V_{OC} losses, too much higher than that of GaAs solar cells, implying a room of 0.1–0.15 V for further improvement on V_{OC}. Better band alignment at the interfaces, lower density of pinholes and local defects, which lead to lower recombination, will benefit for higher V_{OC}. Getting higher shunt resistance and smaller series resistance of the device through interfacial engineering will hold the key for *FF* improvement from currently 0.78–0.83 to > 0.85, close to that of GaAs solar cells.

If all above criteria are fulfilled, a suggested J_{SC} of 27 mA cm^{-2} (3 mA cm^{-2} loss), V_{OC} of 1.17 eV (0.3 V loss), *FF* of 0.85 could be expected, which could finally give the record efficiency up to 26.85%. This goal is very possible to be achieved in the next 3–5 years.

4.1.2 PCE of PVSC module

From laboratory small cells (<1 cm^2) to PVSC submodules (~ 100 cm^2), it is mostly associated with process scale up in thin film technologies. The spin-coating method commonly employed in laboratory is not feasible in the production line. Uniform and pin-hole free perovskite film with designed pattern is the most important layer in comparison to the other interfacial charge transport layers, because the former is totally new while the latter has already been sufficiently studied in other photoelectric fields.

Some feasible processes to prepare high quality large area perovskite films are summarized in Figure 7. (1) $MAPbI_3$ thin film can be prepared by PbI_2-MAI two sources thermal evaporation reported by Liu et al. (Figure 7(a)) [85]. The films are pin-hole-free and highly uniform in a large area. Though it has been reported with a 15.4% efficiency with a regular planar cell structure, the later followers found it was really hard to get a satisfied performance [138]. It is thought beyond morphological control, some unknown defects have been embedded in the evaporated perovskite film, which cannot be identified from XRD detection but is detrimental to the device performance. (2) Doctor-blading (Figure 7(b))/slot die coating (Figure 7(d)) are the most commonly used techniques in organic solar cells [139–143] owing to the process simpleness and cost-effectiveness. Both of them have been demonstrated to achieve acceptably high performance of PVSCs (10.14%–15.1%). The problem is that it is difficult to tune the viscosity of the binder-free perovskite paste; therefore, normally a fast curing process during coating is required. As demonstrated by Kyeongil et al. [144], during slot-die coating, the *in-situ* N_2 gas blow-dry played a decisive role in the pin-hole free morphology of the as-prepared $MAPbI_3$ film (Figure 7(d)) [144,145]. (3) Spray-deposition is an easy method to fabricate large-area uniform films, but it can hardly realize the surface roughness and the full coverage on the substrate (Figure 7(c) [146], Figure 7(e) [147]). Besides, the toxic precursor should be strictly confined in a closed chamber. As demon-

Table 2 Comparison of the performance parameters (including the theoretical maximum values) among the best PVSCs and commercialized mono-Si, CIGS, GaAs solar cells

	The best PVSCs		Mono-Si	CIGS	GaAs
	$FAPbI_3$ [48]	$MAPbI_3$ [22]			
Bandgap (eV)	1.47	1.55	1.1	1.14	1.43
V_{OC} (V)	1.059	1.083	0.740	0.757	1.122
V_{OC} deficit (V)	0.411	0.467	0.36	0.343	0.308
J_{SC} upper limit	29.39	26.83	43.7	43.7	31.6
J_{SC} (mA cm^{-2})	24.65	20.43	41.8	35.7	29.68
FF (%)	77	82.7	82.7	77.6	86.5
PCE (%)	20.1	18.3	25.6	21.0	28.8

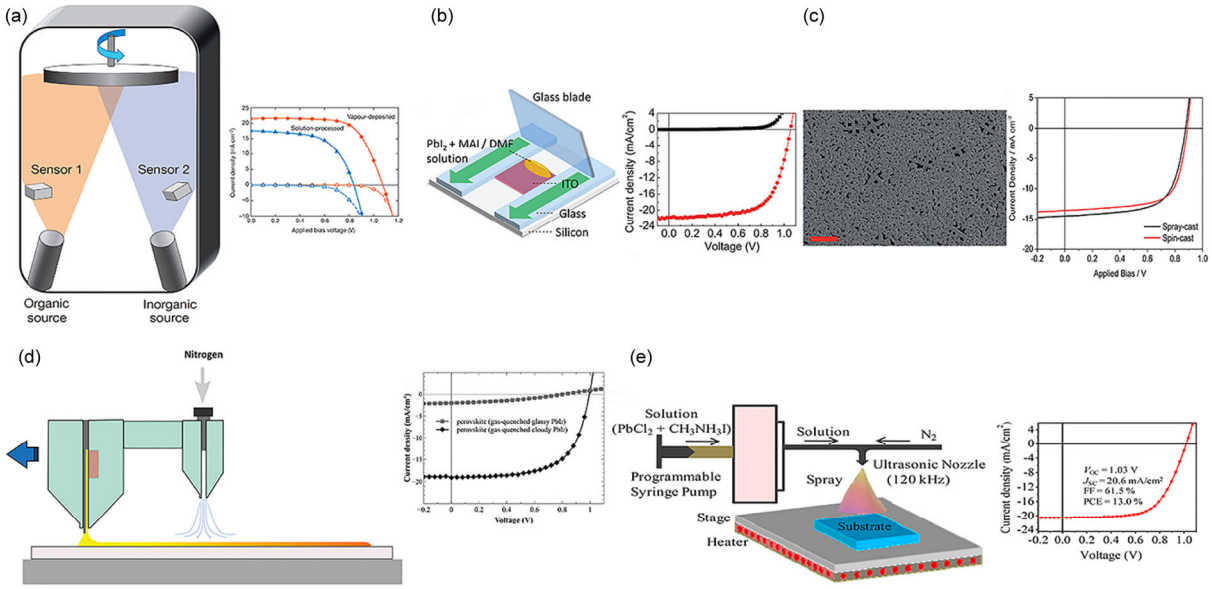

Figure 7 (Color online) The reported strategies suitable for fabrication of large area perovskite films: (a) vapor deposition [85]; (b) doctor-blading [139]; (c) thermal spray deposition [146]; (d) slot-die coating [144]; (e) ultrasonic spray deposition [147].

strated by Sanjib et al. [147], the temperature of the substrate during spray- casting, the volatility of the casting solvent and the post deposition anneal all have impacts on the device performance [146–148].

In comparison to the complexity of the c-Si and CIGS solar cell production lines, PVSCs could be produced much simpler definitely. That is because the light absorber, perovskites, the most important component in photovoltaic devices, are solution processable at low temperature. The efficiency of large area PVSC module catches up with the laboratory efficiency of small cells is only a matter of time.

4.2 Stability

Stability is the toughest obstacle before PVSCs could be really accepted by the PV market. According to the highest level of stability standards for organic solar cells [149], a qualified product needs to pass all of the dark, outdoor, lab weathering, thermal cycling, solar-thermal-humidity tests, as summarized in Table 3. To current stage of PVSCs, possibly only dark/65°C is close to be resolved if the encapsulation quality could be good enough. Others stability tests have been tried and acceptable results at more mild conditions have been achieved [22,150,151]. However, to pass all of those tests under conditions listed in Table 3 at the same time is still facing great challenge.

Not only long-term stability issues have not been resolved, many fresh PVSCs as reported in the literatures even cannot give short-term stable power output within minutes [105]. Referring to Keith Emery, the manager of the National Renewable Energy Laboratory's (NREL) photovoltaic cell and module performance characterization group in the US, the instability of PVSCs is reflected as the rapid degradation as soon as they are tested [152]. From this, one may understand why no one before Chen et al. [22] (the corresponding author of this paper) reported a certified high efficiency from the five credible PV certification centers, like NREL in the US and AIST in Japan, which are listed as the affiliations in the formal "solar cell efficiency tables" [18–21,122].

The inherent reasons responsible for instability of PVSCs include: (1) the degradation of the organo-metal halides, which related to their weak bonding energies and crystal formation energies. Perovskites are reported to be sensitive to temperature, moisture, light exposure and bias potential [153]. Ionic motion beyond direct decomposition of perovskites is more likely to occur in the solar cells under the working conditions, even if the device is well encapsulated. In fact, PbI_2 is a good ionic conductor with activation energy of only 0.2–0.3 eV for I^- vacancies' motion [154]. Xiao et al. [155] gave strong evidence at first to demonstrate ionic motion in perovskite films, which results in a temporary polarity-switchable solar cell from an initially ohmic and non-rectifying structure (PEDOT:PSS/$MAPbI_3$/Au). The ionic motion of MA^+ in $MAPbI_3$ has been also directly demonstrated recently by Leguy et al. [156] using *in-situ* TEM observation (Figure 8(a)). It is said the collective realignment of MA^+ could screen a device's built-in potential and reduce photovoltaic performance. Yet other ionic defects like I^- and Pb^{2+} as suggested also have the chance to move if given some external energy input. Composition engineering on perovskites, like $[HC(NH_2)_2]_{0.83}Cs_{0.17}Pb(I_{0.6}Br_{0.4})_3$ recently reported by David et al. [57] or perovskite with additive of alkylphosphonic acid ω-ammonium chlorides reported by Li et al. (Figure 8(b)) [150], may hold the key to resolve the intrinsic instability of perovskites. (2)

Table 3 The conditions of stability tests according to organic solar cells international standards [149]

	Dark	Outdoor	Lab, weathering	Thermal cycling	Solar-ther, -hum
Light source	None	Sunlight	Simulator, 1sun	None	Simulator, 1sun
Temperature	65/85°C	Ambient	65/85°C	–40 to +85°C	–25 and 65°C
Humidity	85%	Ambient	Near 50%	Near 55%	50%
Load	V_{OC}	MPP	MPP	V_{OC}	MPP or V_{OC}

Some instable interfacial materials have been involved in the device structure. Note that the well-studied $MAPbI_3$ and $FAPbI_3$ are actually strong Lewis acid. It will react with many unstable interfacial materials, some of which are frequently reported in organic solar cells, such as ZnO [157], Cs_2CO_3 etc. For ZnO interfacial layer, some researchers held a contrary view, claiming that it was very stable [158]. The debate on this point will be clarified very soon. To date, the reported devices with better stability include the printable mesoscopic device of "meso-TiO_2/meso-ZrO_2/meso-Carbon" [124] and the inverted planar device based on inorganic charge extraction layers of "NiMgLiO/perovskite/PCBM/Ti(Nb)O_x" (Figure 8(c)) [22]. The inherent reason should be attributed to the elimination of instable interfacial materials in these cell structures. Besides, recent literatures reflected the efficient interfacial charge extraction was also important for the device stability. Any charge accumulation at the interface would accelerate performance degradation [159].

4.3 Cost

Low cost is another notable advantage of PVSCs. PV module cost consists of materials cost and processing cost. If all of the interfacial materials could be fabricated at low temperature just like perovskites, it is very feasible to produce PVSCs in a roll-to-roll production line. As is known, roll-to-roll printing has been widely used in newspaper printing and has been demonstrated successfully in the production of organic solar modules [160]. As such, the associated processing cost could be extremely low [161]. Roll-to-roll printing PVSCs have recently been demonstrated with validity by Kyeongil et al. [144]. The material cost covers the costs of TCO glass substrates, perovskites light absorbers, interfacial materials, metal electrodes, and sealing materials, etc. It is largely dependent upon the device structure and materials selection. An extremely low-cost design with structure of "ITO/NiO_x/perovskite/ZnO/Al" has been raised by You et al. [158]. In such a device, all of the materials' cost, except ITO, should be very low. A cost analysis on roll-to-roll manufacture of organic solar modules has been reported in 2014 [161]. As predicted by this report, the module cost could be decreased from 34.56 € per m^2 in production line with kW capacity, to 3.63 € per m^2 and to 1.81 € per m^2 for production line with MW and GW capacity. As the photo-active materials, perovskites are much cheaper than that in organic solar cells, and the efficiency record of PVSCs is about two times higher than that of organic solar cells, so the module cost per Wp of PVSCs could be expected to be at least two times lower. Assuming a 10% (short-term task) and 18% (long-term task) module efficiency, the perovskite solar module could be as low as 0.13–0.07 RMB/Wp. That would be more than 10 times lower than that of the current multicrystalline-Si solar modules produced in GW production lines.

4.4 Toxicity

Most of the reported highly efficient PVSCs are based on perovskites containing lead, a well-known toxic element. Especially, the organo-metal halides perovskites have certain solubility in polar solvents, like water from the rain, which increases the concern about the toxicity issue for scale-up application of PVSCs. This is not like the case of Cd in CdTe cells or Pb in PZT of piezo technology, which has been chemically bonded in their crystalline structures and has much lower water-solubility. How to take the toxic issue is still under debate [78]. Some researchers believe there is a very small chance for a perovskite solar panel to leak during its life-cycle. The possibility could be minimized by robust encapsulation of the solar panel or covering the ground underneath the solar panel with plastic sheets. If considering a worst-case scenario accident, a 1 m^2 solar panel with a 300-nm thick $MAPbI_3$ layer would only leak 0.4 g of lead to the soil, which would increase the lead concentration in the first cm of ground below the panel to around 70 ppm. While one should know the typical lead level in soil is 50–200 ppm or even higher in urban areas.

Nevertheless, identifying lead-free alternatives would be very important for further PVSCs development. Several groups have made promising progress in this direction. Especially for pure Sn based perovskites, a group in Northwest Univ. in the US has reported efficiency up to 5.73% (Figure 9(a)) [41]. However, many researchers found it was very hard to repeat such high performance of Sn based PVSCs [162–169]. One commonly recognized problem is the easy oxidization of Sn^{2+} to Sn^{4+}, which in terms of self-doping will largely increase the trap density and therefore decrease the effective diffusion length of the perovskite film [39]. Ge^{2+} based perovskites and Bi^{3+} based perovskites have also been reported, however, the performance were poor(with the best of ~1% PCE) (Figure 9(b) [170] and (c) [171]). Similar to Sn^{2+}, Ge^{2+} could be easily oxidized to Ge^{4+} in air, leading to self-doping of the perovskite film and poor

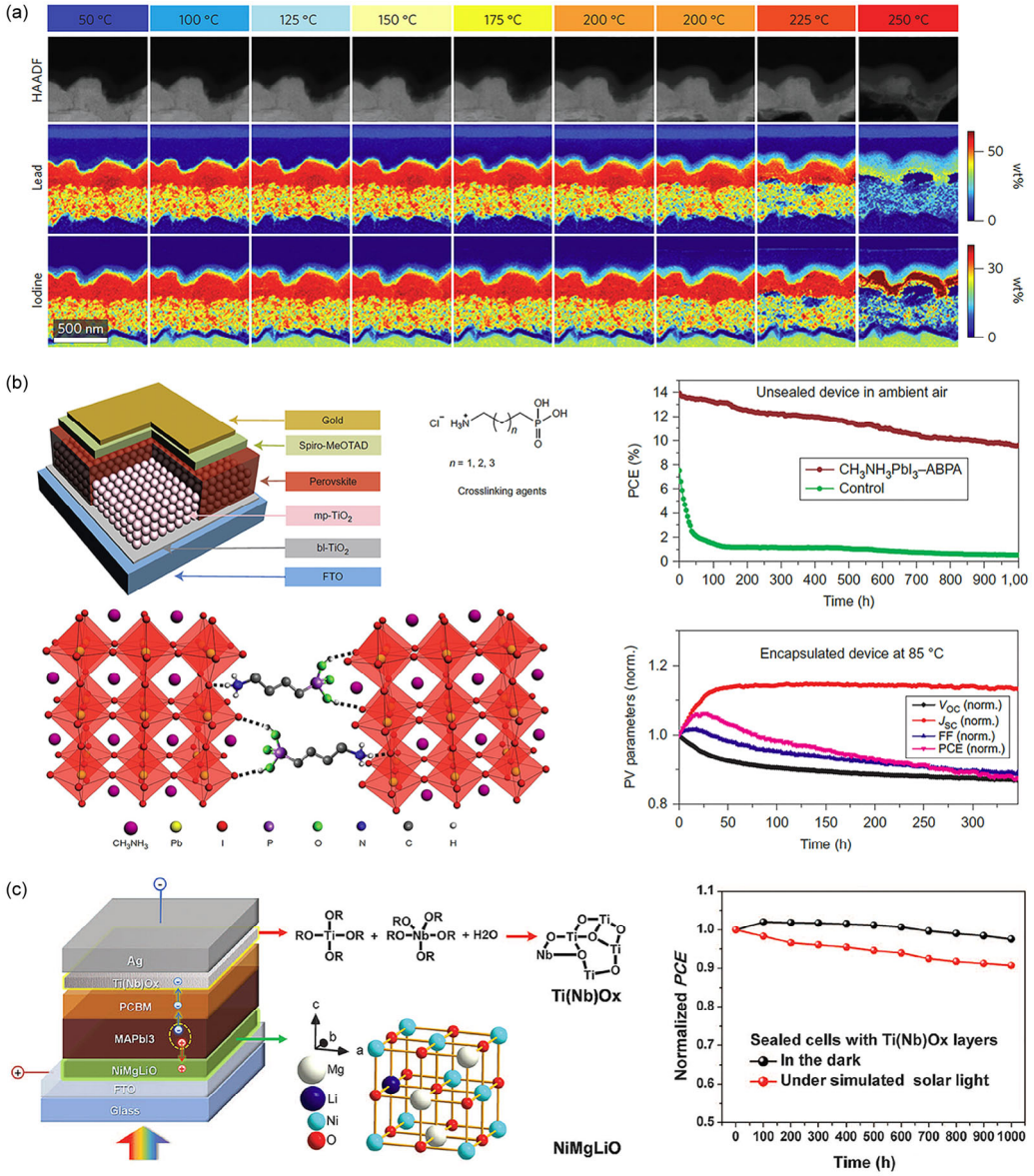

Figure 8 (a) The first *in-situ* observation on head-induced degradation of PVSCs [156]; (b) improved stability of regular mesoscopic PVSCs based on perovskite with additive of alkylphosphonic acid ω-ammonium chlorides [150]; (c) long-term light soaking stability of inverted PVSC based on inorganic charge extraction layers [22].

device performance [170]. While Bi based perovskites have lower symmetry in crystal structure than the Pb based reference, which is suggested to be the inherent reason responsible for the corresponding poor performance of the device [171].

4.5 Short-term industrialization prospects

Indeed, if efficiency, stability, cost, and toxicity have been simultaneously revolved, PVSCs would become a strong competitor to current commercialized PV technologies and even lead to PV market revolution. If the four tasks could not be completely resolved immediately, could PVSCs find any chance to share a certain PV market? The possibility is present if perovskite solar module is endowed with some specific features different from c-Si solar cells. First, PVSCs could be fabricated for the application as semi-transparent and colorful power windows, the feasibility of which has already been demonstrated in laboratory [172,173]. This will facilitate building integrated PV applications, because the power windows can not only behave like a sun-shade but also can generate electricity. An example of power windows made of transparent dye-sensitized solar modules is shown in Figure 10(a) [174]. In the contrast, c-Si solar modules are non-transparent and can only be equipped on the roofs of the buildings, which are scarce resources in China. Second, PVSCs can be made on flexible substrates. Flexibility and portability are notable features for

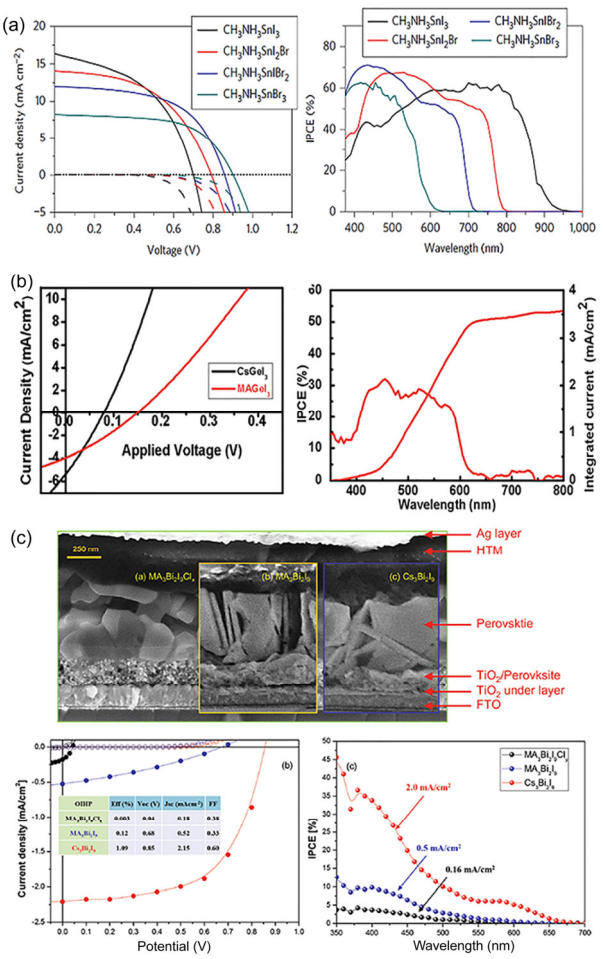

Figure 9 (a) $MASnBr_xI_{3-x}$ based PVSCs: the *I-V* curves (left) and IPCE spectra (right) [41]; (b) $CsGeI_3$ and $MAGeI_3$ based PVSCs: *I-V* curves (left) and IPCE of $MAGeI_3$ (right) [170]; (c) $MA_3Bi_2I_9Cl_x$, $MA_3Bi_2I_9$, $Cs_3Bi_2I_9$ based PVSCs: their cross-section SEM images (top), *I-V* curves (bottom left) and IPCE spectra (bottom right) [171].

certain applications, such as wearable and portable powers required for many civilian and military roles. Several examples employing flexible organic solar cells are shown in Figure 10(b) [175].

5 Conclusion

Low-cost and high efficiency endorse the emerging PVSCs be very attractive alternative to today's commercialized PV technologies. Research effort to this field has an amazing growth in the past few years. At the current stage, it is worthy to review the main achievements in the past and the remaining obstacles in this field. To clarify the embedded reasons responsible for the achievements and obstacles is very important for the next step research and development of PVSCs.

Excellent light absorption and charge transport properties of organo-metal halides perovskites make PVSCs succeed

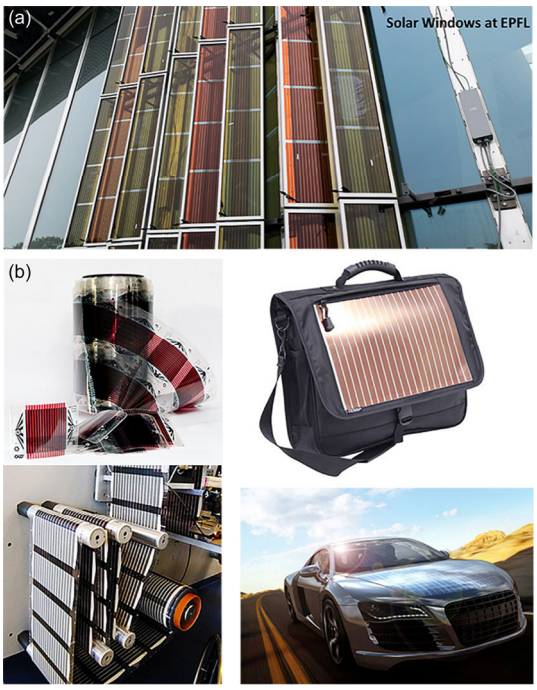

Figure 10 (a) Colorful solar windows made of semi- transparent dye-sensitized solar modules by Gratzel's group at EPFL [174]; (b) roll-to-roll manufactured flexible organic solar modules, integrated with a bag and a car [175].

in achieving outstanding PCE records within a short period of time. Both regular and inverted cell configurations have been demonstrated with very high performance, in which the am-bipolar and balanced charge transport between electrons and holes in perovsiktes played a very important role. The regular cell structure still needs a meso-TiO_2 scaffold to balance charge transport and remove hysteresis. However, the inverted cell structure without any mesoporous scaffold is easier to give hysteresis free *I-V* curves. In principle, any mesoscopic interface would enlarge the possibility of interfacial recombination. It is thought the inverted planar PVSCs with simplified interfacial conditions would quickly catch up with the regular mesoscopic PVSCs in the near future.

A roadmap for PVSCs towards industrialization has been drawn. To further promote module PCE, enhance stability, reduce toxicity, and reduce materials/processing costs should be systematically considered and comprehensively resolved. It is suggested that the semi-transparent and colorful power windows and flexible modules may be the short-term application directions for PVSCs. Any breakthroughs in commercialized applications of PVSCs will attract intensive early-stage investment. According to Wikipedia, the start-up companies have already promised perovskite modules on the market by 2017 [176].

1 U S Energy Information Administration. Monthly Energy Review December 2015. 2015

2 Richard P, Marc P. A fundamental look at energy reserves for the planet. IEA/SHC Solar Update, 2009
3 The United Nations Economic Commission for Europe (UNECE), REN21. UNECE Renewable Energy Status Report, 2015
4 Gribov B G, Zinov'ev K V. Preparation of high-purity silicon for solar cells. Inorg Mater, 2003, 39: 653–662
5 IEA (International Energy Agency). Renewable Energy Medium-Term Market Report. IEA Technical Report, 2014
6 Kavlak G, McNerney J, Jaffe R L, et al. Metal production requirements for rapid photovoltaics deployment. Energy Environ Sci, 2015, 8: 1651–1659
7 Sergio P. Solar grade silicon as a potential candidate material for low-cost terrestrial solar cells. Sol Energy Mater, 1982, 6: 253–297
8 Nada Z. First international workshop on durability and degradation issues in PEM electrolysis cells and its components. Photovoltaics Report, 2013
9 Max M, Armin R. Future recycling flows of tellurium from cadmium telluride photovoltaic waste. Resour Conserv Recycl, 2012, 69: 35–49
10 Rickard A, Duncan K, Sverker M, et al. Energy and resource use assessment of graphene as a substitute for indium tin oxide in transparent electrodes. J Clean Prod, 2015, doi: 10.1016/j.jclepro.2015.04.076
11 Michael R, Roderick E, Michael W. Evaluating the availability of gallium, indium, and tellurium from recycled photovoltaic modules. Sol Energy Mater Sol Cells, 2015, 138: 58–71
12 Green Technology Media (Gtm) Research. February 2009: CIGS Thin-Film Manufacturing Players and Cost Models. 2009
13 Solar Power World online. Building better solar cells. http://www.solarpowerworldonline.com/2010/09/making-better-solar-cells/, 2010
14 Gregory P, Claire M, Terry G. Indium and gallium supply sustainability September 2007 update. In: 22nd EU PV Solar Conference, Milan, Italy, 2007
15 Neelkanth G D. Toward GW/year of CIGS production within the next decade. Sol Energy Mater Sol Cells, 2007, 91: 1376–1382
16 Christian K. CIGS-Baseline. https://www.helmholtzbelin.de/projects/pvcomb/forschen/cigs_en.html, 2014
17 NREL. Best research-cell efficiencies. http://www.nrel.gov/ncpv/images/efficiency_chart.jpg, 2015
18 Martin A G, Keith E, Yoshihiro H, et al. Solar cell efficiency tables (Version 43). Prog Photovoltaics, 2014, 22: 1–9
19 Martin A G, Keith E, Yoshihiro H, et al. Solar cell efficiency tables (Version 44). Prog Photovoltaics, 2014, 22: 701–710
20 Martin A G, Keith E, Yoshihiro H, et al. Solar cell efficiency tables (Version 45). Prog Photovoltaics, 2015, 23: 1–9
21 Martin A G, Keith E, Yoshihiro H, et al. Solar cell efficiency tables (Version 47). Prog Photovoltaics, 2016, 24: 3–11
22 Chen W, Wu Y Z, Han L Y, et al. Efficient and stable large-area perovskite solar cells with inorganic charge extraction layers. Science, 2015, 350: 944–948
23 3Dciencia. Perovskite. https://3dciencia.wordpress.com/2013/01/25/perovskite/, 2013
24 Rosner H, Weht R, Johannes M D, et al. Superconductivity near Ferromagnetism in $MgCNi_3$. Phys Rev Lett, 2001, 88: 027001
25 Bannikov V V, Shein I R, Ivanovskii A L. Electronic structure, chemical bonding and elastic properties of the first thorium-containing nitride perovskite $TaThN_3$. Phys Status Solidi-Rapid Res Lett, 2007, 1: 89–91
26 Ewa R, Dag N, Karim K, et al. Investigation of the perovskite related structures of $NaMgH_3$, $NaMgF_3$ and Na_3AlH_6. J Alloy Compd, 2000, 299: 101–106
27 Chen Q, Nicholas D M, Yang Y, et al. Under the spotlight: The organic–inorganic hybrid halide perovskite for optoelectronic applications. Nano Today, 2015, 10: 355–396
28 Pena M A, Fierro J L G. Chemical structures and performance of perovskite oxides. Chem Rev, 2001, 101: 1981–2017
29 Li C H, Lu X, Guo Z M, et al. Formability of ABX_3 (X = F, Cl, Br, I) halide perovskites. Acta Crystallogr Sect B-Struct Sci Cryst Eng Mat, 2008, 64: 702–707
30 Glazer A M. The classification of tilted octahedra in perovskites. Acta Crystallogr Sect B-Struct Sci Cryst Eng Mat, 1972, B28: 3384–3392
31 David B M. Templating and structural engineering in organic–inorganic perovskites. J Chem Soc, 2001. 1–12
32 Liu X C, Hong R Z, Tian C S. Tolerance factor and the stability discussion of ABO_3-type ilmenite. J Mater Sci-Mater Electron, 2009, 20: 323–327
33 Li C H, Kitty C K S, Wu P. Formability of ABO_3 perovskites. J Alloy Compd, 2004, 372: 40–48
34 Martin A G, Anita H, Henry J S. The emergence of perovskite solar cells. Nat Photonics, 2014, 8: 506–514
35 Zhang Y B, Tsung-Ta T, Wang F, et al. Direct observation of a widely tunable bandgap in bilayer grapheme. Nature, 2009, 459: 820–823
36 Ni Z Y, Liu Q, Lu J, et al. Tunable bandgap in silicene and germanene. Nano Lett, 2012, 12: 113–118
37 Jun H N, Sang H I, Sang Il S, et al. Chemical management for colorful, efficient, and stable inorganic–organic hybrid nanostructured solar cells. Nano Lett, 2013, 13: 1764–1769
38 Samrana K, Mohammad K N, Shahzada A, et al. Perovskite as light harvester: A game changer in photovoltaics. Angew Chem Int Ed, 2014, 53: 2812–2824
39 Nakita K N, Samuel D S, Henry J S, et al. Lead-free organic–inorganic tin halide perovskites for photovoltaic applications. Energy Environ Sci, 2014, 7: 3061–3068
40 Belen S, Victoria G P, Ivan M S. Recombination study of combined halides (Cl, Br, I) perovskite solar cells. J Phys Chem Lett, 2014, 5: 1628–1635
41 Hao F, Constantinos C S, Mercouri G K, et al. Lead-free solid-state organic–inorganic halide perovskite solar cells. Nat Photonics, 2014, 8: 489–494
42 Hao F, Constantinos C S, Mercouri G K, et al. Anomalous band gap behavior in mixed Sn and Pb perovskites enables broadening of absorption spectrum in solar cells. J Am Chem Soc, 2014, 136: 8094–8099
43 Shockley W, Queisser H J. Detailed balance limit of efficiency of p-n junction solar cells. J Appl Phys, 1961, 32: 510
44 Eperon G E, Stranks S D, Menelaou C, et al. Formamidinium lead trihalide: A broadly tunable perovskite for efficient planar heterojunction solar cells. Energy Environ Sci, 2014, 7: 982
45 Colella S, Mosconi E, Fedeli P, et al. $MAPbI_{3-x}Cl_x$ mixed halide perovskite for hybrid solar cells: The role of chloride as dopant on the transport and structural properties. Chem Mat, 2013, 25: 4613–4618
46 Kulkarni S A, Baikie T, Boix P P, et al. Band-gap tuning of lead halide perovskites using a sequential deposition process. J Mater Chem A, 2014, 2: 9221–9225
47 Eperon G E, Stranks S D, Menelaou C, et al. Formamidinium lead trihalide: a broadly tunable perovskite for efficient planar heterojunction solar cells. Energy Environ Sci, 2014, 7: 982–988
48 Yang W S, Noh J H, Jeon N J, et al. High-performance photovoltaic perovskite layers fabricated through intramolecular exchange. Science, 2015, 348: 1234–1237
49 Amat A, Mosconi E, Ronca E, et al. Cation-induced band-gap tuning in organohalide perovskites: interplay of spin-orbit coupling and octahedra tilting. Nano Lett, 2014, 14: 3608–3616
50 Yuhei O, Atsushi M, Shuzi H, et al. $CH_3NH_3Sn_xPb_{(1-x)}I_3$ Perovskite Solar Cells Covering up to 1060 nm. J Phys Chem Lett, 2014, 5: 1004–1011
51 Ziya K, Tugba O, Engin U A, et al. Tetrastyryl-BODIPY-Based dendritic light harvester and estimation of energy transfer efficiency. Org Lett, 2012, 14: 3636–3639
52 Wen F Y, Wang X L, Li C. A Hybrid photocatalytic system comprising ZnS as light harvester and an $[Fe_2S_2]$ hydrogenase mimic as hydrogen evolution catalyst. ChemSusChem, 2012, 5: 849–853
53 Guo X Z, Luo Y H, Meng Q B, et al. Can the incident pho-

to-to-electron conversion efficiency be used to calculate short-circuit current density of dye-sensitized solar cells. Curr Appl Phys, 2012, 12: e54–e58
54 Henry J S. Perovskites: The emergence of a new era for low-cost, high-efficiency solar cells. J Phys Chem Lett, 2013, 4: 3623–3630
55 Dou L T, You J B, Yang Y, et al. Tandem polymer solar cells featuring a spectrally matched low-bandgap polymer. Nat Photonics, 2012, 6: 180–185
56 Chen C W, Hsiao S Y, Lin H W, et al. Optical properties of organometal halide perovskite thin films and general device structure design rules for perovskite single and tandem solar cells. J Mater Chem A, 2015, 3: 9152–9159
57 David P M, Golnaz S, Henry J S, et al. A mixed-cation lead mixed-halide perovskite absorber for tandem solar cells. Science, 2016, 351: 151–155
58 Xing G C, Nripan M, Tze C S, et al. Long-range balanced electron- and hole-transport lengths in organic-inorganic $CH_3NH_3PbI_3$. Science, 2013, 342: 344–347
59 Samuel D S, Giles E E, Henry J S, et al. Electron-hole diffusion lengths exceeding 1 micrometer in an organometal trihalide perovskite absorber. Science, 2013, 342: 341-344
60 Giacomo G, Hiroshi S, Koichi Y, et al. Small photocarrier effective masses featuring ambipolar transport in methylammonium lead iodide perovskite: A density functional. J Phys Chem Lett, 2013, 4: 4213–4216
61 Carlito S P J, Tom J S, Villy S, et al. Organometal halide perovskite solar cell materials rationalized: ultrafast charge generation, high and microsecond-long balanced mobilities, and slow recombination. J Am Chem Soc, 2014, 136: 5189–5192
62 Zhao Y X, Alexandre M N, Zhu K. Solid-state mesostructured perovskite $CH_3NH_3PbI_3$ solar cells: charge transport, recombination, and diffusion length. J Phys Chem Lett, 2014, 5: 490–494
63 Dong Q F, Fang Y J, Huang J S, et al. Electron-hole diffusion lengths > 175 μm in solution-grown $CH_3NH_3PbI_3$ single crystals. Science, 2015, 347: 967–970
64 Dar M I, Arora N, Gao P, et al. Investigation regarding the role of chloride in organic–inorganic halide perovskites obtained from chloride containing precursors. Nano Lett, 2014, 14: 6991–6996
65 Chen Q, Zhou H, Yang Y, et al. The optoelectronic role of chlorine in $CH_3NH_3PbI_3$(Cl)-based perovskite solar cells. Nat Commun, 2015, 6: 7269
66 Colella S, Mosconi E, Pellegrino G, et al. Elusive presence of chloride in mixed halide perovskite solar cells. J Phys Chem Lett, 2014, 5: 3532–3538
67 Zhao Y, Zhu K. CH_3NH_3Cl-Assisted one-step solution growth of $CH_3NH_3PbI_3$: structure, charge-carrier dynamics, and photovoltaic properties of perovskite solar cells. J Phys Chem C, 2014, 118: 9412–9418
68 Chang J, Zhu H, Li B, et al. Boosting the performance of planar heterojunction perovskite solar cell by controlling the precursor purity of perovskite materials. J Mater Chem A, 2016, 4: 887–893
69 Liu F, Dong Q, Wong M K, et al. Is excess PbI_2 beneficial for perovskite solar cell performance?. Adv Energy Mater, 2016, 6: 1502206
70 Chen Q, Zhou H, Song T B, et al. Controllable self-induced passivation of hybrid lead iodide perovskites toward high performance solar cells. Nano Lett, 2014, 14: 4158–4163
71 Kim Y C, Jeon N J, Noh J H, et al. Beneficial effects of PbI_2 Incorporated in organo-lead halide perovskite solar cells. Adv Energy Mater, 2016, 6: 1502104
72 Bi D, Ahmed M El-Z, Hagfeldt A, et al. Unraveling the effect of PbI_2 concentration on charge recombination kinetics in perovskite solar cells. ACS Photonics, 2015, 2: 589–594
73 Sharenko A, Toney M F. Relationships between lead halide perovskite thin-film fabrication, morphology, and performance in solar cells. J Am Chem Soc, 2016, 138: 463–470
74 Eperon G E, Burlakov V M, Docampo P, et al. Morphological control for high performance, solution-processed planar heterojunction perovskite solar cells. Adv Funct Mater, 2014, 24: 151–157
75 Li W, Fan J, Li J, et al. Controllable grain morphology of perovskite absorber film by molecular self-assembly toward efficient solar cell exceeding 17%. J Am Chem Soc, 2015, 137: 10399–10405
76 Ahn N, Son D Y, Jang I H, et al. Highly reproducible perovskite solar cells with average efficiency of 18.3% and best efficiency of 19.7% fabricated via lewis base adduct of lead (ii) iodide. J Am Chem Soc, 2015, 137: 8696–8699
77 Bergmann V W, Weber S A, Javier R F, et al. Real-space observation of unbalanced charge distribution inside a perovskite-sensitized solar cell. Nat Commun, 2014, 5: 5001
78 Noh J H, Sang Il S. Steps toward efficient inorganic–organic hybrid perovskite solar cells. MRS Bull, 2015, 40: 648-653
79 Heo J H, You M S, Chang M H, et al. Hysteresis-less mesoscopic $CH_3NH_3PbI_3$ perovskite hybrid solar cells by introduction of li-treated TiO_2 electrode. Nano Energy, 2015, 15: 530–553
80 Brown G, Faifer V, Pudov A, et al. Determination of the minority carrier diffusion length in compositionally graded Cu(In, Ga)Se_2 solar cells using electron beam induced current. Appl Phys Lett, 2010, 96: 022104
81 Ettenberg M. Minority carrier diffusion length and recombination lifetime in GaAs:Ge prepared by liquid-phase epitaxy. J Appl Phys, 1973, 44: 827
82 Khedher N, Hajji M, Bouaïcha M, et al. Improvement of transport parameters in solar grade monocrystalline silicon by application of a sacrificial porous silicon layer. Solid State Commun, 2002, 123: 7–10
83 Bi D, Tress W, Dar M I, et al. Efficient luminescent solar cells based on tailored mixed-cation perovskites. Sci Adv, 2016, 2: e1501170
84 Zhou H P, Chen Q, Yang Y, et al. Interface engineering of highly efficient perovskite solar cells. Science, 2014, 345: 542–546
85 Liu M Z, Michael B J, Henry J S. Efficient planar heterojunction perovskite solar cells by vapour deposition. Nature, 2013, 501: 395–398
86 Pablo D, James M B, Mariam D, et al. Efficient organometal trihalide perovskite planar-heterojunction solar cells on flexible polymer substrates. Nat Commun, 2013, 4: 2761
87 Jeng J Y, Chiang Y F, Lee M H, et al. $CH_3NH_3PbI_3$ perovskite/fullerene planar-heterojunction hybrid solar cells. Adv Mater, 2013, 25: 3727–3732
88 Xiao Z G, Bi C, Shao Y C, et al. Efficient, high yield perovskite photovoltaic devices grown by interdiffusion of solution-processed precursor stacking layers. Energy Environ Sci, 2014, 7: 2619–2623
89 Nie W Y, Hsinhan T, Aditya D M, et al. High-efficiency solution-processed perovskite solar cells with millimeter-scale grains. Science, 2015, 347: 522–525
90 Wu C G, Chiang C H, Tseng Z L, et al. High efficiency stable inverted perovskite solar cells without current hysteresis. Energy Environ Sci, 2015, 8: 2725–2733
91 Wang K C, Shen P S, Guo T F, et al. Low-temperature sputtered nickel oxide compact thin film as effective electron blocking layer for mesoscopic NiO/$CH_3NH_3PbI_3$ perovskite heterojunction solar cells. ACS Appl Mater Interfaces, 2014, 6: 11851–11858
92 Wang K C, Jeng K Y, Wen T C, et al. p-type Mesoscopic nickel oxide/organometallic perovskite heterojunction solar cells. Sci Rep, 2014, 4: 4756
93 Jeng J Y, Chen K C, Hsu Y J, et al. Nickel oxide electrode interlayer in $CH_3NH_3PbI_3$ perovskite/pcbm planar-heterojunction hybrid solar cells. Adv Mater, 2014, 26: 4107–4113
94 Zhu Z L, Bai Y, Yang S H, et al. High-performance hole-extraction layer of sol–gel-processed NiO nanocrystals for inverted planar perovskite solar cells. Angew Chem Int Ed, 2014, 126: 12779–12783
95 Chen W, Wu Y Z, Han L Y, et al. Hybrid interfacial layer leads to solid performance improvement of inverted perovskite solar cells. Energy Environ Sci, 2015, 8: 629–640
96 Jong H P, Jangwon S, Sang Il S, et al. Efficient $CH_3NH_3PbI_3$ per-

ovskite solar cells employing nanostructured p-Type NiO electrode formed by a pulsed laser deposition. Adv Mater, 2015, 27: 4013–4019
97 Jae W J, Chueh C C, Alex K Y J. A low-temperature, solution-processable, Cu-Doped nickel oxide hole-transporting layer via the combustion method for high-performance thin-film perovskite solar cells. Adv Mater, 2015, 27: 7874–7880
98 Kojima A, Teshima K, Shirai Y, et al. Organometal halide perovskites as visible-light sensitizers for photovoltaic cells. J Am Chem Soc, 2009, 131: 6050–6051
99 Kim H S, Lee C R, Im J H, et al. Lead iodide perovskite sensitized all-solid-state submicron thin film mesoscopic solar cell with efficiency exceeding 9%. Sci Rep, 2012, 2: 591
100 Julian B, Norman P, Michael G, et al. Sequential deposition as a route to high-performance perovskite-sensitized solar cells. Nature, 2013, 499: 316–319
101 Nam J J, Jun H N, Sang Il S, et al. Solvent engineering for high-performance inorganic–organic hybrid perovskite solar cells. Nat Mater, 2014, 13: 897–903
102 Nam J J, Jun H N, Sang Il S, et al. Compositional engineering of perovskite materials for high-performance solar cells. Nature, 2015, 517: 476–480
103 Michael M L, Joël T, Henry J S. Efficient hybrid solar cells based on meso-superstructured organometal halide perovskites. Science, 2012, 338: 643–647
104 Henry J S, Antonio A, James M B, et al. Anomalous hysteresis in perovskite solar cells. J Phys Chem Lett, 2014, 5: 1511–1515
105 Zhang Y, Liu M Z, Henry J S, et al. Charge selective contacts, mobile ions and anomalous hysteresis in organic–inorganic perovskite solar cells. Mater Horiz, 2015, 2: 315-322
106 Chen H W, Nobuya S, Tsutomu M. Emergence of hysteresis and transient ferroelectric response in organo-lead halide perovskite solar cells. J Phys Chem Lett, 2015, 6: 164–169
107 Jarvist M F, Keith T B, Aron W. Molecular ferroelectric contributions to anomalous hysteresis in hybrid perovskite solar cells. APL Mater, 2014, 2: 081506
108 Wu B, Fu K, Yantara N, et al. Charge accumulation and hysteresis in perovskite-based solar cells: An electro-optical analysis. Adv Energy Mater, 2015, 5: 1500829
109 Wang Q, Ito S, Gratzel M, et al. Characteristics of high efficiency dye-sensitized solar cells. J Phys Chem B, 2006, 110: 25210–25221
110 Shin S S, Yang W S, Noh J H, et al. High-performance flexible perovskite solar cells exploiting Zn_2SnO_4 prepared in solution below 100 degrees. Nat Commun, 2015, 6: 7410
111 Henry J S, Grätzel M. Electron and hole transport through mesoporous tio2 infiltrated with spiro-OMeTAD. Adv Mater, 2007, 19: 3643–3647
112 Yip H L, Jen A K Y. Recent advances in solution-processed interfacial materials for efficient and stable polymer solar cells. Energy Environ Sci, 2012, 5: 5994
113 Chen S, Manders J R, Tsang S W, et al. Metal oxides for interface engineering in polymer solar cells. J Mater Chem, 2012, 22: 24202
114 Subbiah A S, Halder A, Ghosh S, et al. Inorganic hole conducting layers for perovskite-based solar cells. J Phys Chem Lett, 2014, 5: 1748–1753
115 Hu L, Peng J, Wang W, et al. Sequential deposition of $CH_3NH_3PbI_3$ on planar NiO film for efficient planar perovskite solar cells. ACS Photonics, 2014, 1: 547–553
116 Cui J, Meng F, Zhang H, et al. $CH_3NH_3PbI_3$-based planar solar cells with magnetron-sputtered nickel oxide. ACS Appl Mater Interfaces, 2014, 6: 22862–22870
117 Zhao Y, Nardes A M, Zhu K. Effective hole extraction using moox-al contact in perovskite $CH_3NH_3PbI_3$ solar cells. Appl Phys Lett, 2014, 104: 213906
118 Ren Z, Ng A, Shen Q, et al. Thermal assisted oxygen annealing for high efficiency planar $CH_3NH_3PbI_3$ perovskite solar cells. Sci Rep, 2014, 4: 6752
119 Spiccia L, Xiao M, Gao M, et al. Efficient perovskite solar cells employing inorganic interlayers. Chem Nano Mat, 2016, doi: 10.1002/cnma.201500223
120 Li Z. Stable perovskite solar cells based on WO_3 nanocrystals as hole transport layer. Chem Lett, 2015, 44: 1140–1141
121 Kim J H, Liang P W, Williams S T, et al. High-performance and environmentally stable planar heterojunction perovskite solar cells based on a solution-processed copper-doped nickel oxide hole-transporting layer. Adv Mater, 2015, 27: 695–701
122 Green M A, Emery K, Hishikawa Y, et al. Solar cell efficiency tables (version 46). Prog Photovoltaics, 2015, 23: 805–812
123 Sessolo M, Bolink H J. Perovskite solar cells join the major league. Science, 2015, 350: 917
124 Mei A Y, Li X, Han H W, et al. A hole-conductor–free, fully printable mesoscopic perovskite solar cell with high stability. Science, 2014, 345: 295–298
125 Li X, Tschumi M, Han H, et al. Outdoor performance and stability under elevated temperatures and long-term light soaking of triple-layer mesoporous perovskite photovoltaics. Energy Technol, 2015, 3: 551–555
126 Xu X B, Liu Z H, Wang M K, et al. Hole selective NiO contact for efficient perovskite solar cells with carbon electrode. Nano Lett, 2015, 15: 2402–2408
127 Wei Z, Chen H, Yan K, et al. Inkjet printing and instant chemical transformation of a $CH_3NH_3PbI_3$/nanocarbon electrode and interface for planar perovskite solar cells. Angew Chem Int Ed, 2014, 126: 13455–13459
128 Wei Z, Yan K, Chen H, et al. Cost-efficient clamping solar cells using candle soot for hole extraction from ambipolar perovskites. Energy Environ Sci, 2014, 7: 3326–3333
129 Wei Z, Chen H, Yan K, et al. Hysteresis-free multi-walled carbon nanotube-based perovskite solar cells with a high fill factor. J Mater Chem A, 2015, 3: 24226–24231
130 Chen H, Wei Z, Yan K, et al. Liquid phase deposition of TiO_2 nanolayer affords $CH_3NH_3PbI_3$/nanocarbon solar cells with high open-circuit voltage. Faraday Discuss, 2014, 176: 271–286
131 Chen H, Wei Z, Zheng X, et al. A scalable electrodeposition route to the low-cost, versatile and controllable fabrication of perovskite solar cells. Nano Energy, 2015, 15: 216–226
132 Chen H, Wei Z, He H, et al. Solvent engineering boosts the efficiency of paintable carbon-based perovskite solar cells to beyond 14%. Adv Energy Mater, 2016, 6: 1502087
133 Ko D H, Tumbleston J R, Gadisa A, et al. Light-trapping nano-structures in organic photovoltaic cells. J Mater Chem, 2011, 21: 16293
134 Hua B, Lin Q, Zhang Q, et al. Efficient photon management with nanostructures for photovoltaics. Nanoscale, 2013, 5: 6627–6640
135 Xiao Z, Dong Q, Bi C, et al. Solvent annealing of perovskite-induced crystal growth for photovoltaic-device efficiency enhancement. Adv Mater, 2014, 26: 6503–6509
136 Scharber M C, Mühlbacher D, Koppe M, et al. Design rules for donors in bulk-heterojunction solar cells—towards 10 % energy-conversion efficiency. Adv Mater, 2006, 18: 789–794
137 Chen Q, Zhou H P, Yang Y, et al. Planar heterojunction perovskite solar cells via vapor-assisted solution process. J Am Chem Soc, 2014, 136: 622–625
138 Tavakoli M M, Gu L, Gao Y, et al. Fabrication of efficient planar perovskite solar cells using a one-step chemical vapor deposition method. Sci Rep, 2015, 5: 14083
139 Deng Y H, Edwin P, Huang J S, et al. Scalable fabrication of efficient organolead trihalide perovskite solar cells with doctor-bladed active layers. Energy Environ Sci, 2015, 8: 1544–1550
140 Aldo D C, Francesco D G, Silvia L, et al. Mesoscopic perovskite solar cells and modules. In: Proceedings of the 14th IEEE International Conference on Nanotechnology, Toronto, Canada, 2014
141 Francesco D G, Francesco D G, Aldo D C, et al. Solid-state solar modules based on mesoscopic organometal halide perovskite: A route towards the up-scaling process. Phys Chem Chem Phys, 2014, 16: 3918–3923
142 Razza S, Di Giacomo F, Matteocci F, et al. Perovskite solar cells and

large area modules (100 cm^2) based on an air flow-assisted pbi2 blade coating deposition process. J Power Sources, 2015, 277: 286–291
143 Yang M J, Zhou Y Y, Zhu K, et al. Square-centimeter solution-processed planar $CH_3NH_3PbI_3$ perovskite solar cells with effi ciency exceeding 15%. Adv Mater, 2015, 27: 6363–6370
144 Kyeongil H, Jung Y S, Doojin V, et al. Toward large scale roll-to-roll production of fully printed perovskite solar cells. Adv Mater, 2015, 27: 1241–1247
145 Martin K, Getachew A, Martin K, et al. Flexible high power-per-weight perovskite solar cells with chromium oxide–metal contacts for improved stability in air. Nat Mater, 2015, 14: 1032–1039
146 Alexander T B, Andrew J P, David G L, et al. Efficient planar heterojunction mixed-halide perovskite solar cells deposited via spray-deposition. Energy Environ Sci, 2014, 7: 2944–2950
147 Sanjib D, Yang B, Xiao K, et al. High-performance flexible perovskite solar cells by using a combination of ultrasonic spray-coating and low thermal budget photonic curing. ACS Photonics, 2015, 2: 680–686
148 Luis K O, Wang S H, Qi Y B. Fabrication of semi-transparent perovskite films with centimeter-scale superior uniformity by the hybrid deposition method. Energy Environ Sci, 2014, 7: 3989–3993
149 Reese M O, Gevorgyan S A, Jørgensen M, et al. Consensus stability testing protocols for organic photovoltaic materials and devices. Sol Energy Mater Sol Cells, 2011, 95:1253–1267
150 Li X, Dar M I, Yi C, et al. Improved performance and stability of perovskite solar cells by crystal crosslinking with alkylphosphonic acid omega-ammonium chlorides. Nat Chem, 2015, 7: 703–711
151 Tomas L, Giles E E, Henry J S, et al. Overcoming ultraviolet light instability of sensitized TiO_2 with meso-superstructured organometal tri-halide perovskite solar cells. Nat Commun, 2013, 4: 2885
152 Gunther M. Meteoric rise of perovskite solar cells under scrutiny over efficiencies. http://wwwrscorg/chemistryworld/2015/02/meteoritic-rise-perovskite-solar-cells-under-scrutiny-over-efficiencies, 2015
153 Han Y, Meyer S, Dkhissi Y, et al. Degradation observations of encapsulated planar $CH_3NH_3PbI_3$ perovskite solar cells at high temperatures and humidity. J Mater Chem A, 2015, 3: 8139–8147
154 Mizusaki J, Arai K, Fueki K. Ionic conduction of the perovskite-type halides. Solid State Ion, 1983, 11: 203–211
155 Xiao Z, Yuan Y, Shao Y, et al. Giant switchable photovoltaic effect in organometal trihalide perovskite devices. Nat Mater, 2015, 14: 193–198
156 Leguy A M, Frost J M, McMahon A P, et al. The dynamics of methylammonium ions in hybrid organic-inorganic perovskite solar cells. Nat Commun, 2015, 6: 7124
157 Cheng Y, Yang Q D, Xiao J, et al. Decomposition of organometal halide perovskite films on zinc oxide nanoparticles. ACS Appl Mater Interfaces, 2015, 7: 19986–19993
158 You J B, Meng L, Yang Y, et al. Improved air stability of perovskite solar cells via solution-processed metal oxide transport layers. Nat Nanotechnol, 2016, 11: 75–81
159 Zhao Y, Liang C, Zhang H, et al. Anomalously large interface charge in polarity-switchable photovoltaic devices: An indication of mobile ions in organic–inorganic halide perovskites. Energy Environ Sci, 2015, 8: 1256–1260
160 Søndergaard R, Hösel M, Angmo D, et al. Roll-to-roll fabrication of polymer solar cells. Mater Today, 2012, 15: 36–49
161 Machui F, Hösel M, Li N, et al. Cost analysis of roll-to-roll fabricated ito free single and tandem organic solar modules based on data from manufacture. Energy Environ Sci, 2014, 7: 2792
162 He Y, Galli G. Perovskites for solar thermoelectric applications: A first principle study of $CH_3NH_3AI_3$ (A = Pb and Sn). Chem Mat, 2014, 26: 5394–5400
163 Feng J, Xiao B. Effective masses and electronic and optical properties of nontoxic $MASnX_3$ (X = Cl, Br, and I) perovskite structures as solar cell absorber: A theoretical study using HSE06. J Phys Chem C, 2014, 118: 19655–19660
164 Camille B, Kesong Y. First-principles hybrid functional study of the organic–inorganic perovskites $CH_3NH_3SnBr_3$ and $CH_3NH_3SnI_3$. J Phys Chem C, 2014, 118: 24383–24388
165 Hao F, Stoumpos C C, Guo P, et al. Solvent-mediated crystallization of $CH_3NH_3SnI_3$ films for heterojunction depleted perovskite solar cells. J Am Chem Soc, 2015, 137: 11445–11452
166 Umari P, Mosconi E, De A F. Relativistic gw calculations on $CH_3NH_3PbI_3$ and $CH_3NH_3SnI_3$ perovskites for solar cell applications. Sci Rep, 2014, 4: 4467
167 Zuo F, Williams S T, Liang P W, et al. Binary-metal perovskites toward high-performance planar-heterojunction hybrid solar cells. Adv Mater, 2014, 26: 6454-6460
168 Mulmudi H K, Dharani S, Nripan M, et al. Lead-free halide perovskite solar cells with high photocurrents realized through vacancy modulation. Adv Mater, 2014, 26: 7122–7127
169 Alessandro S, Domenico D S, Silvia P, et al. Tunable ferroelectric polarization and its interplay with spin–orbit coupling in tin iodide perovskites. Nat Commun, 2014, 5: 5900
170 Thirumal K, Ding C H D, Subodh G M, et al. Lead-free germanium iodide perovskite materials for photovoltaic applications. J Mater Chem A, 2015, 3: 23829–23832
171 Park B, Philippe B, Zhang X, et al. Bismuth based hybrid perovskites $A_3Bi_2I_9$ (A: Methylammonium or Cesium) for solar cell application. Adv Mater, 2015, 27: 6806–6813
172 Bryant D, Greenwood P, Troughton J, et al. A transparent conductive adhesive laminate electrode for high-efficiency organic-inorganic lead halide perovskite solar cells. Adv Mater, 2014, 26: 7499–7504
173 You P, Liu Z, Tai Q, et al. Efficient semitransparent perovskite solar cells with graphene electrodes. Adv Mater, 2015, 27: 3632–3638
174 Herzog A. Epfl's campus has the world's first solar window. https://actuepflch/news/epfl-s-campus-has-the-world-s-first-solar-window/, 2005
175 Tek R. The next great leap forward in power technology to be powered by organic photovoltaics. http://www.raynergytek.com/ index.asp, 2014
176 Oxford P V. Reveals breakthrough in efficiency of new class of solar cell. http://www.oxfordpv.com/oxford-pv-news/oxford-pv-reveals-breakthrough-in-efficiency-of-new-class-of-solar-cell/, 2013